REVIEW

Triboelectric Nanogenerators

ADVANCED
ENERGY
MATERIALS

www.advenergymat.de

Triboelectric Nanogenerator: A Foundation of the Energy for the New Era

Changsheng Wu, Aurelia C. Wang, Wenbo Ding, Hengyu Guo, and Zhong Lin Wang*

As the world is marching into the era of the internet of things (IoTs) and artificial intelligence, the most vital development for hardware is a multifunctional array of sensing systems, which forms the foundation of the fourth industrial revolution toward an intelligent world. Given the need for mobility of these multitudes of sensors, the success of the IoTs calls for distributed energy sources, which can be provided by solar, thermal, wind, and mechanical triggering/vibrations. The triboelectric nanogenerator (TENG) for mechanical energy harvesting developed by Z.L. Wang's group is one of the best choices for this energy for the new era, since triboelectrification is a universal and ubiquitous effect with an abundant choice of materials. The development of self-powered active sensors enabled by TENGs is revolutionary compared to externally powered passive sensors, similar to the advance from wired to wireless communication. In this paper, the fundamental theory, experiments, and applications of TENGs are reviewed as a foundation of the energy for the new era with four major application fields: micro/nano power sources, self-powered sensors, large-scale blue energy, and direct high-voltage power sources. A roadmap is proposed for the research and commercialization of TENG in the next 10 years.

1. Introduction of the Triboelectric Nanogenerator (TENG)

1.1. History

The triboelectric effect is ubiquitous in our everyday life and results from two different materials coming into contact. It is generally regarded as a negative effect in industry given that the electrostatic charges induced from it can lead to ignition, dust explosions, dielectric breakdown, electronic damage, etc. From an energy point of view, those electrostatic charges constitute a capacitive energy device when the two triboelectric surfaces are separated, which led to the invention of early electrostatic generators such as the "friction machine" and Van de Graaff generator.[1]

C. Wu, A. C. Wang, Dr. W. Ding, Dr. H. Guo, Prof. Z. L. Wang
School of Materials Science and Engineering
Georgia Institute of Technology
Atlanta, GA 30332, USA
E-mail: zhong.wang@mse.gatech.edu
Prof. Z. L. Wang
Beijing Institute of Nanoenergy and Nanosystems
Chinese Academy of Sciences
Beijing 100083, P. R. China

The ORCID identification number(s) for the author(s) of this article can be found under https://doi.org/10.1002/aenm.201802906.

By coupling this triboelectric effect and electrostatic induction, the TENG was first invented by the Wang group in 2012 (**Figure 1**a) to effectively harness ambient mechanical energy that is ubiquitous but usually wasted in our everyday life.[2] More specifically, triboelectrification/contact electrification provides static polarized charges on material surfaces in contact, while electrostatic induction drives the transformation of mechanical energy to electricity through the change in electrical potential induced by mechanically agitated separation. Over the past six years, this TENG concept has been expanded to different working modes[3–8] to enable broad application scenarios, such as mechanical vibration, human motion, wind, and water waves.[9,10]

In addition to versatile operation modes, the TENG has many other merits, including broad material availability, light weight, low cost, and high efficiency even at low operation frequency. In principle, any material with distinct charge affinity can be used to construct a TENG, which results in a broad range of materials at opposite ends of the triboelectric series capable of high performance. Among them, polytetrafluoroethylene (PTFE) and silicone are commonly used materials for attaining net negative triboelectric charges while nylon and metal are for net positive charges. Most current TENGs are polymer-based and flexible, easy to fabricate, cost-effective, and highly portable,[11] while high-temperature TENGs are built from durable ceramics materials for extreme conditions of operation.[12,13] Moreover, the power density of a TENG, which depends on the device structure and active materials, has been reported to be up to 500 W m^{-2}.[14] The energy harvested using TENGs is sufficient to drive many small electronics and make self-powered electronics networks viable. Given the enormous number of sensors required in the era of Internet of Things (IoTs) and existing environmental concerns associated with battery replacement on a large scale, TENGs will potentially serve as a new alternative energy source of great significance and thus have also been proposed as "the energy for the new era" in 2017.[15]

1.2. Current Status around the Globe

Together with the piezoelectric nanogenerator (PENG) invented by Wang group in 2006, the emerging nanogenerator technology has been widely regarded as a revolution in the field of energy harvesting and sensing, and has yielded about 195 patents.[16] Its

trends, impacts, and strategies toward large-scale commercialization have been studied using various methods,[16–20] such as bibliometrics, patent analysis, tech mining, techno-economic lifetime assessment, and technology road-mapping, with the results showing that nanogenerator development is becoming more interdisciplinary and calls for efforts not only from materials science and nanotechnology, but also from computer science, information systems, public policy, and many others. The international conference on nanogenerators and piezotronics (NGPT) was initiated in 2012 and has been held every two years ever since, with the number of attendees rising from 50 in 2012 to ≈400 in 2018 and the host location switching between North America, Asia, and Europe. A prestigious peer-reviewed journal, Nano Energy, was founded by the inventor of TENGs, Prof. Z. L. Wang in 2012, to promote the development of nanomaterials-related energy solutions, among which the nanogenerator is an important subject. As of now, the TENG has displayed increasingly rapid development and has become the forerunner of growth in the nanogenerator field. The number of TENG-related publications has seen an exponential increase from only 8 in 2012 to about 400 in 2017, with authors hailing from over 40 countries. Several TENG-based commercial products, such as air filters[21] and face masks,[22] have been launched in local markets of China, which pioneer and pave the path toward large-scale commercialization.

1.3. Objectives of This Review

This rapid development in TENGs calls for periodic reviews so that the technology's readiness can be properly evaluated and critical challenges can be addressed in a timely manner. In the past few years, several reviews have summarized the progress of TENG technology in theoretical modeling,[23] energy harvesting,[24–28] and active sensing,[29–31] which provide useful references for researchers in related fields. Meanwhile, several milestones in the fundamental understanding and practical application of TENGs have been reported recently, which allows us to obtain a more comprehensive picture of TENGs from both scientific and practical perspectives. The motivation of this review is not just a summary of what has been achieved, but more importantly, is to provide a guideline for future development. In this review, therefore, a great emphasis is placed on the fundamental understanding of TENG, including its theoretical origins, the triboelectrification mechanism, performance-enhancement factors, standards, and power management strategies. Subsequently, recent important progresses in TENG applications are introduced, with the selection criterion being either universally applicable solutions or pioneering work in a field with huge impact. Furthermore, a road map of TENG research is proposed to identify prioritized directions and provide a timeframe for TENG development.

2. Fundamentals of TENG

2.1. Theoretical Origin and Model of TENG

The first TENG device, whose contact-separation design is still the basis of most current ones, consisted of a polyester (PET) film and Kapton film with back electrodes coated on them

Changsheng Wu received his bachelor of engineering in engineering science from National University of Singapore in 2013. He is currently pursuing a Ph.D. in materials science and engineering at Georgia Institute of Technology under the supervision of Prof. Zhong Lin Wang. His research interests include energy harvesting, self-powered electronics, and additive manufacturing.

Aurelia C. Wang received her BS in biochemistry in 2013 from the Georgia Institute of Technology. After working at Medical Neurogenetics from 2014 to 2016, she returned to the Georgia Institute of Technology to work on her doctoral research under the supervision of Prof. Zhiqun Lin and Prof. Zhong Lin Wang. Her research interests include nanomaterials, polymer-based energy harvesting, and self-powered smart device design.

Zhong Lin (ZL) Wang is the Hightower Chair in Materials Science and Engineering, Regents' Professor, and Engineering Distinguished Professor at Georgia Tech. He is also the chief scientist and director of the Beijing Institute of Nanoenergy and Nanosystems, Chinese Academy of Sciences. His discovery and breakthroughs in nanogenerators establish the principle and technological road map for harvesting mechanical energy from environment and biological systems for powering personal electronics. His research on self-powered nanosystems has inspired worldwide efforts in academia and industry for studying energy for micro-nanosystems, which is now a distinct disciplinary in energy research and future sensor networks.

(Figure 1a).[2] The device could generate AC output when the contact status between the two films changed, that is, when it underwent cyclic pressing or bending motion. The initial explanation of the working mechanism was described in a
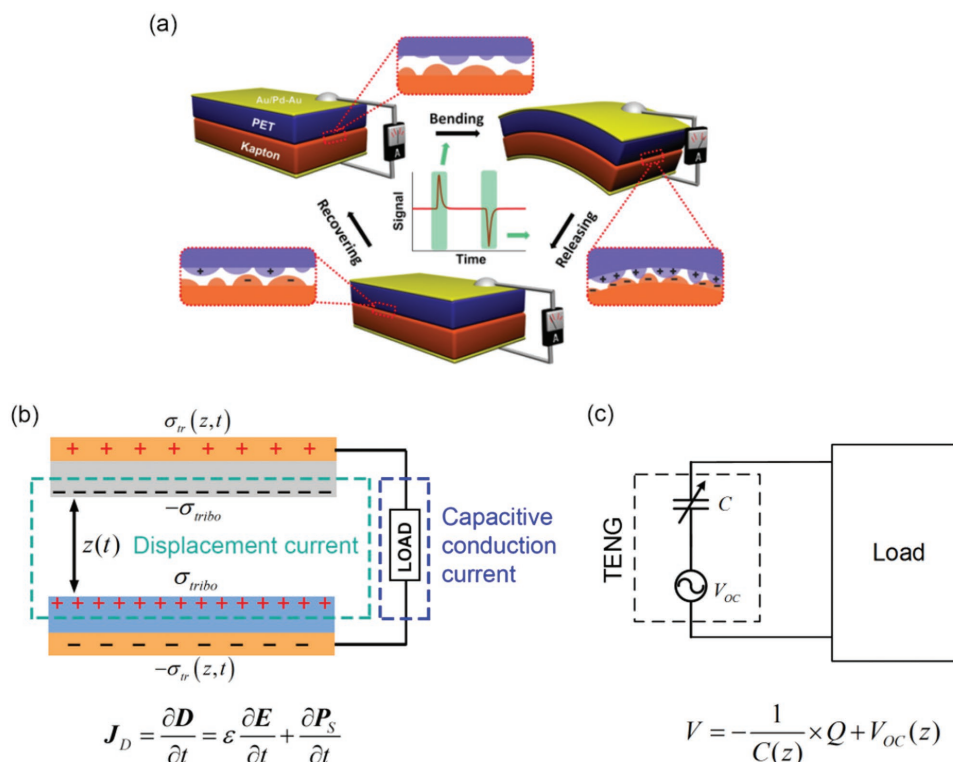
Figure 1. Theoretical models of TENG. a) Schematic illustration of the first TENG and its operation cycle. Reproduced with permission.[2] Copyright 2012, Elsevier. b) The displacement current model of a contact-separation-mode TENG. c) The equivalent electrical circuit model of TENG.

qualitative manner. When the two active triboelectric materials, PET and Kapton, come into contact under pressing or bending, triboelectric charges will be induced on their surfaces. As the external force is released, the charged surfaces will be separated, and an electric potential difference will be built upon the two back electrodes. If the electrodes are connected to external load, current will flow between them to screen out the electric field built up by the charged surfaces. As they are brought into contact again by external mechanical stimuli, the potential difference on the electrodes will change and current will flow back in the opposite direction. A continuous AC output can be obtained by repeating this operation cycle. In other words, the device operates on the coupling of two commonly observed phenomena, contact electrification and electrostatic induction, with the former providing the static polarized charges on material surfaces and the latter driving the transformation of mechanical energy to electricity via mechanically triggered change in electric potential. This qualitative description provides a straightforward understanding of contact separation TENGs, but the fundamental physics model has been lacking until the mechanism origin was traced back to Maxwell's displacement current in 2017.[15,32] Maxwell's displacement current is defined as

$$J_D = \frac{\partial \boldsymbol{D}}{\partial t} = \varepsilon \frac{\partial \boldsymbol{E}}{\partial t} + \frac{\partial \boldsymbol{P}_S}{\partial t} \tag{1}$$

where $\boldsymbol{D}$ is the displacement field, ε is the permittivity of the medium, $\boldsymbol{E}$ is the electric field, and $\boldsymbol{P}_S$ is the polarization

contributed by the presence of surface polarization charges contributed from piezoelectric and or triboelectric effect. The first term refers to a time-varying electric field and is tied to the origin of electromagnetic waves, while the second term presents the contribution from surface polarization and is the origin of nanogenerators. More specifically, in piezoelectric nanogenerators, this polarization comes from piezoelectric polarization charges generated by applied strain. In TENGs, external electrostatic charges induced from triboelectrification build up time-varying surface polarization as two materials in contact undergo mechanically agitated displacement.

The basic model of a contact-separation-mode TENG is illustrated in Figure 1b. It has two electrodes connected to external load and two dielectrics for contact electrification. The dielectric surfaces are oppositely charged due to contact electrification with a surface charge density of $\pm\sigma_{tribo}$, which is saturated after the initial contact cycles and independent of the gap distance z. The triboelectric charges build up an electrostatic field, which drives free electrons to flow through the external load and transfer between the electrodes. The amount of transferred charges accumulated on the electrodes, $\pm\sigma_{tr}$, is a function of z, and thus, the mechanical energy which induces change in z is converted into electrical energy. The corresponding displacement current can be calculated as

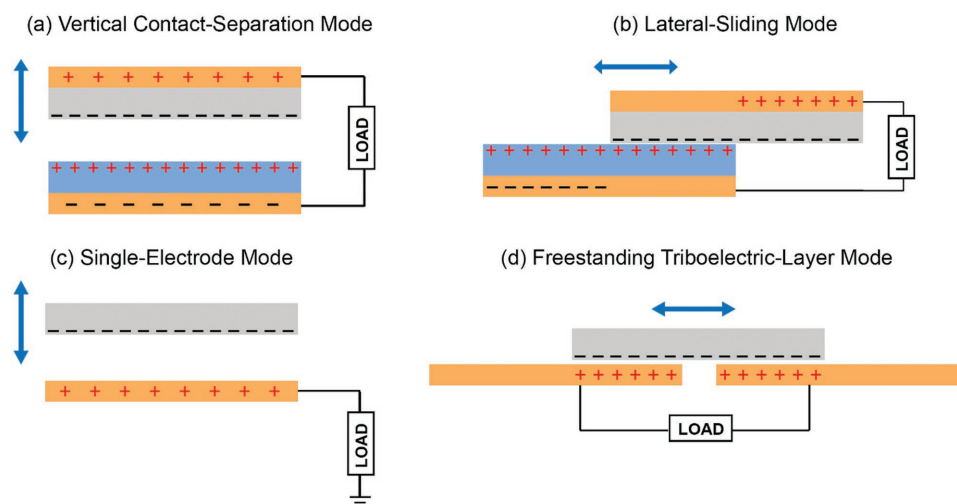$$J_D = \frac{\partial D_z}{\partial t} = \frac{\partial \sigma_{tr}(z,t)}{\partial t} \tag{2}$$

Figure 2. Four working modes of TENG. a) Vertical CS mode. b) LS mode. c) SE mode. d) FT mode.

This displacement current is the only conduction mechanism for electricity transport in capacitive conduction and leads to the output current of TENG via electromagnetic waves and induction, rather than the flow of free charges directly across the electrodes as in a resistor.

Oppositely charged surfaces with a changing gap distance can be viewed as a capacitor with varying capacitance. This perspective gives a more intuitive representation of the TENG using the capacitor model (Figure 1c), whose current is given by

$$I = \frac{dQ}{dt} = A\frac{d\sigma_{tr}}{dt} \tag{3}$$

The result is equivalent to Equation (2) and validates that Maxwell's displacement current is the foundation of the capacitive model. The corresponding output voltage of TENG can be written as

$$V = -\frac{1}{C(z)} \times Q + V_{OC}(z) \tag{4}$$

Along with Ohm's law, this capacitive model of TENG is the theoretical tool that enables the study, design, and optimization of TENG.[33–38] Another model using the distance-dependent electric field concept and Norton's theorem has also been proposed recently to more accurately simulate the output behavior of a TENG with an external load.[39,40] However, it should be emphasized that Maxwell's displacement current is the fundamental basis for all of these detailed electrical models.

2.2. Four Working Modes of TENG

Depending on the direction of the polarization change and electrode configuration, four different operation modes of the TENG have been proposed since its first report in 2012, including vertical contact-separation (CS) mode, lateral-sliding

(LS) mode, single-electrode (SE) mode, and freestanding triboelectric-layer (FT) mode, as shown in **Figure 2**.[3] The vertical CS mode uses relative motion perpendicular to the interface, and the potential change between electrodes and thus external current flow is dictated by the gap distance between material surfaces. The lateral-sliding mode uses the relative displacement in the direction parallel to the interface, and it can be implemented in a compact package via rotation-induced sliding. The single-electrode mode takes the ground as the reference electrode and is versatile in harvesting energy from a freely moving object without attaching an electric conductor, such as a hand typing, human walking, and moving transportation. The freestanding triboelectric-layer mode is developed upon the single-electrode mode, but instead of using the ground as the reference electrode, it uses a pair of symmetric electrodes and electrical output is induced from asymmetric charge distribution as the freely moving object changes its position. One thing worth noting is that practical application of TENG is not limited to one single mode, but relies more on conjunction or hybridization of different modes to harness their full advantages. The theoretical models of all four modes have been extensively studied and reviewed in previous publications, and thus are not covered in detail here.[23] Since TENG devices commonly operate in a hybrid mode, the applications of TENGs will not be discussed based on the operation mode but on the application scenario in Section 3.

2.3. Figure of Merits (FOM) of TENG

The four working modes and the vast variety of applicable materials of TENG call for a common standard so that the performance of different TENGs can be compared and evaluated. The milestone work of a specialized figure of merit for TENG was reported by Zi et al. in 2015, in which a performance figure of merit (FOM_P) for TENG consisting of a structural FOM (FOM_S) and a material FOM (FOM_M) was proposed.[41] The FOM_P is used to characterize the performance of a TENG, just like the efficiency for solar cells and the *ZT* factor for thermoelectric materials.
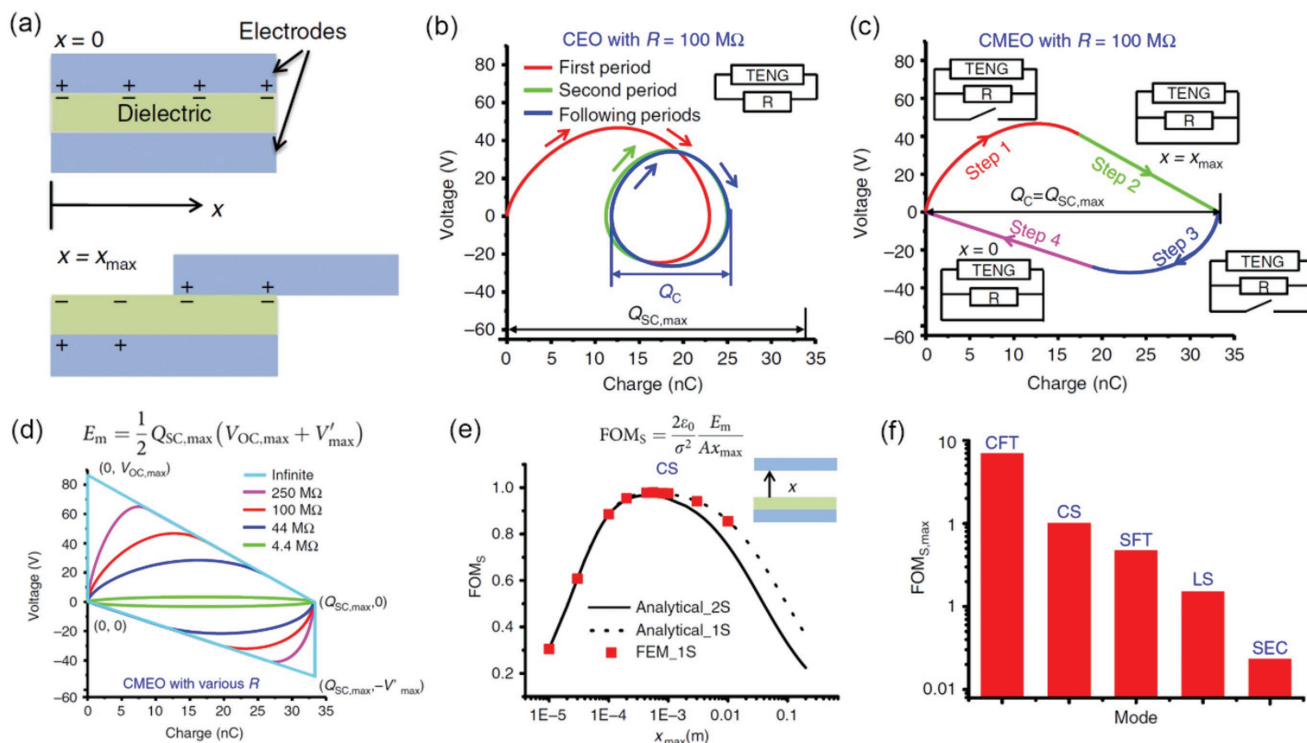
Figure 3. Figure of merits for TENG. a) Schematic of the LS mode TENG. b) The CEO of the LS mode TENG with a load resistance of 100 MΩ. c) The CMEO of the LS mode TENG with a load resistance of 100 MΩ. d) The CMEO of the LS mode TENG with various load resistances. e) The FOM$_S$ for a vertical CS-mode TENG versus x_{max}. f) The maximum FOM$_S$ (FOM$_{S,max}$) for different working modes calculated from FEM simulations. Reproduced under the terms of the CC-BY 4.0 license.[41] Copyright 2015, Springer Nature.

The authors initiated the study by investigating the output behavior of a LS mode TENG, with its schematic shown in **Figure 3**a. The plots of the built-up voltage V against the transferred charges Q under various load resistance were simulated using the finite element method (FEM), with the results for 100 MΩ shown in Figure 3b. The enclosed area in the V–Q plot represents the output energy per cycle, and thus the V–Q cycles are named as cycles for energy output (CEO). The TENG operation is known to reach a steady state, that is, closed V–Q loops, after a certain number of operation cycles, and the steady-state CEO will differ with different external load resistance. The total cycling charge Q_C is defined as the difference between the maximum and the minimum transferred charges in a steady-state CEO and is noted to be smaller than the maximum transferred charges $Q_{SC,max}$ under short-circuit conditions (Figure 3b). Therefore, new cycles for maximized energy output (CMEO) are proposed by employing instantaneous short-circuit conditions during TENG operation so that $Q_C = Q_{SC,max}$ can be achieved (Figure 3c). The TENG is connected to the external load resistance during step 1 and step 3, while the displacement between triboelectric materials changes from $x = 0$ to $x = x_{max}$, and vice versa. During step 2 and step 4, the switch in parallel with the external load is turned on to enable the transferred charges Q to reach $Q_{SC,max}$ and 0, respectively. The CMEOs for various load resistances are shown in Figure 3d, indicating a maximized energy output per cycle E_m at $R = +\infty$. The equation for calculating E_m is expressed as

$$E_m = \frac{1}{2}Q_{SC,max}\left(V_{OC,max} + V'_{max}\right) \tag{5}$$

where $Q_{SC,max}$, $V_{OC,max}$, and V'_{max} are all proportional to the triboelectric charge density σ. Given that the average output power and energy-conversion efficiency at the CMEO are proportional to E_m/x_{max}, a dimensionless structural FOM is proposed as

$$FOM_S = \frac{2\varepsilon_0}{\sigma^2 A}\frac{E_m}{x_{max}} \tag{6}$$

where ε_0 is the permittivity of vacuum and A the triboelectrification area of TENG. The term $\sigma^2 A$ is introduced in the denominator so that the effects of material properties and device size are excluded in the FOM$_S$. Consequently, the performance FOM is defined as

$$FOM_P = FOM_S \cdot \sigma^2 = \frac{2\varepsilon_0}{A}\frac{E_m}{x_{max}} \tag{7}$$

where σ^2 can be defined as the FOM$_M$. As seen from Equation (6), the FOM$_S$ is dependent on the maximum displacement x_{max} and can be optimized by adjusting the value of x_{max} (Figure 3e). The FOM$_{S,max}$ for different working modes of a TENG is summarized in Figure 3f, giving the relationship CFT > CS > SFT > LS > SEC, where CFT stands for contact FT mode, SFT for sliding FT, and SEC for SE contact mode.

ADVANCED
SCIENCE NEWS
www.advancedsciencenews.com

ADVANCED
ENERGY
MATERIALS
www.advenergymat.de

A standard method for quantifying the triboelectric performance of a material is proposed as well. The triboelectric charge density of the test material with respect to a certain liquid metal such as Galinstan is measured. A dimensionless material FOM is defined by normalizing the triboelectric charge density from the test material with that from a reference material such as fluorinated ethylene propylene (FEP)

$$\mathrm{FOM_{DM}} = (\sigma_N)^2 = \frac{\sigma^2_{Material/Galinstan}}{\sigma^2_{FEP/Galinstan}} \tag{8}$$

The use of liquid metal rather than solid materials is justified by the more intimate contact of a liquid–solid interface and thus less influence of surface roughness. A negative σ_N means the material is more triboelectrically positive than Galinstan, and a σ_N larger than one means it is more triboelectrically negative than FEP, and something in between means it is more negative than Galinstan but more positive than FEP.

2.4. Charge Transfer Mechanism in Contact Electrification

The displacement current model, the capacitive model, and figure of merits of TENG all suggest that its output current and voltage are proportional to the triboelectric surface charge density, and that the output power is proportional to the square of charge density. However, the origin of the triboelectric charges, or the underlying mechanism of contact-electrification, is still unclear, especially when insulating or polymer materials are involved. Previous studies have suggested that electron or ion transfer is involved but the debate about which is the dominant mechanism persists.[42–45] Recently, Xu et al. investigated this age-old problem by using the TENG as a characterization tool for surface electrostatic charges, which enabled them to quantitatively study the temporal evolution of surface charge density at different temperatures.[12] They reported that electron transfer, rather than ion transfer, dominates the contact electrification process between insulators due to the consistency between their results and the electron thermionic emission model. They also proposed an electron-cloud-potential-well model that potentially explains the contact-electrification process between all types of materials.

To investigate the temperature-dependency of surface charges, the authors fabricated high-temperature CS-mode TENGs consisting of different material pairs, such as Ti-SiO$_2$ and Ti-Al$_2$O$_3$. The initial surface charges on SiO$_2$ or Al$_2$O$_3$ were generated by rubbing them with polyurethane foam, and the surface charge density retained on SiO$_2$/Al$_2$O$_3$ at different temperatures and times was characterized by the amount of charge transferred per TENG operation cycle. This is possible because the contact-electrification process between Ti and SiO$_2$/Al$_2$O$_3$ during TENG operation generates limited surface charges compared to the initial charge generation process between SiO$_2$/Al$_2$O$_3$ and polyurethane, and thus induces negligible effect on the output charge transfer. The measurement setup with the Ti-SiO$_2$ TENG is illustrated in **Figure 4**a and the temporal evolution of its output charge transfer Q_{SC} at various temperatures is summarized in Figure 4b. The results indicate that the increase in temperature induces faster decay in surface charge, and

more importantly, the decay follows an exponential trend with respect to time under high temperatures except for the first few minutes (inset of Figure 2b). This decay trend fits well with the electron thermionic emission model, which is depicted by

$$J = \lambda A_0 T^2 e^{-\frac{W}{kT}} \left[e^{\frac{\Delta W}{kT}} - 1 \right] \tag{9}$$

where J is the current density, λ the material-specific correction factor, A_0 the Richardson constant of a free electron, T the temperature, W the height of the potential barrier, k the Boltzmann constant, and ΔW the potential barrier height variation due to the surface electric field E.

With the assumption of $\Delta W \propto E \propto Q_{SC}$ and $\Delta W \ll kT$ as well as the relationship $J = \frac{1}{A}\frac{dQ_{SC}}{dt}$, the thermionic emission equation leads to an exponential decay in surface charge, similar to their experimental data

$$Q_{SC} = e^{-SAt} Q_{SC0} \tag{10}$$

where A is the surface area, S the temperature-dependent factor, and Q_{SC0} the initial value of Q_{SC}. The imperfect fit or slow decay trend during the initial few minutes is attributed to temperature destabilization and is not observed in the case of Ti-Al$_2$O$_3$ thanks to the faster thermal equilibrium from the enhanced thermal conductivity and thinner thickness of Al$_2$O$_3$. More evidence that the authors provided for the electron-transfer-dominated mechanism is the comparison of the charge decay rate after treating the TENG in contact or separation status to a high temperature of 473 K. The decay rate is slower when the Ti-SiO$_2$ surfaces are in contact, which is contradictory to previous ion transfer model by Harper.[46]

An electron-cloud-potential-well model was also proposed to explain the electron-transfer-dominant mechanism of contact-electrification (Figure 4c). Initially (i), the two materials A and B with different highest occupied energy levels are separated with a distance between electron clouds of d, and the electrons are trapped in their respective potential wells. When the materials are in contact, the electron clouds will overlap and electrons will flow from A to B (ii), and most of the transferred electrons will stay in B even after the separation of the materials, resulting in positively charged A and negatively charged B (iii). With the increase in temperature, transferred electrons in B are more likely to hop out of the potential well and be thermionically emitted, inducing surface charges decay (iv). This work is a milestone fundamental work on contact electrification by providing a new investigative approach to studying TENGs and similarly, also giving invaluable insights on TENG development, especially on high-temperature design and strategies in output improvement.

2.5. Strategies for Improving Triboelectric Charge Density

Numerous research efforts on TENG performance improvement have been devoted to increasing the triboelectric charge density, which dictates the output voltage, current, and power. These endeavors can be classified into three strategies: modification in material composition, improvement in effective contact area, and change in environmental conditions (**Figure 5**). The material

ADVANCED
SCIENCE NEWS
www.advancedsciencenews.com

ADVANCED
ENERGY
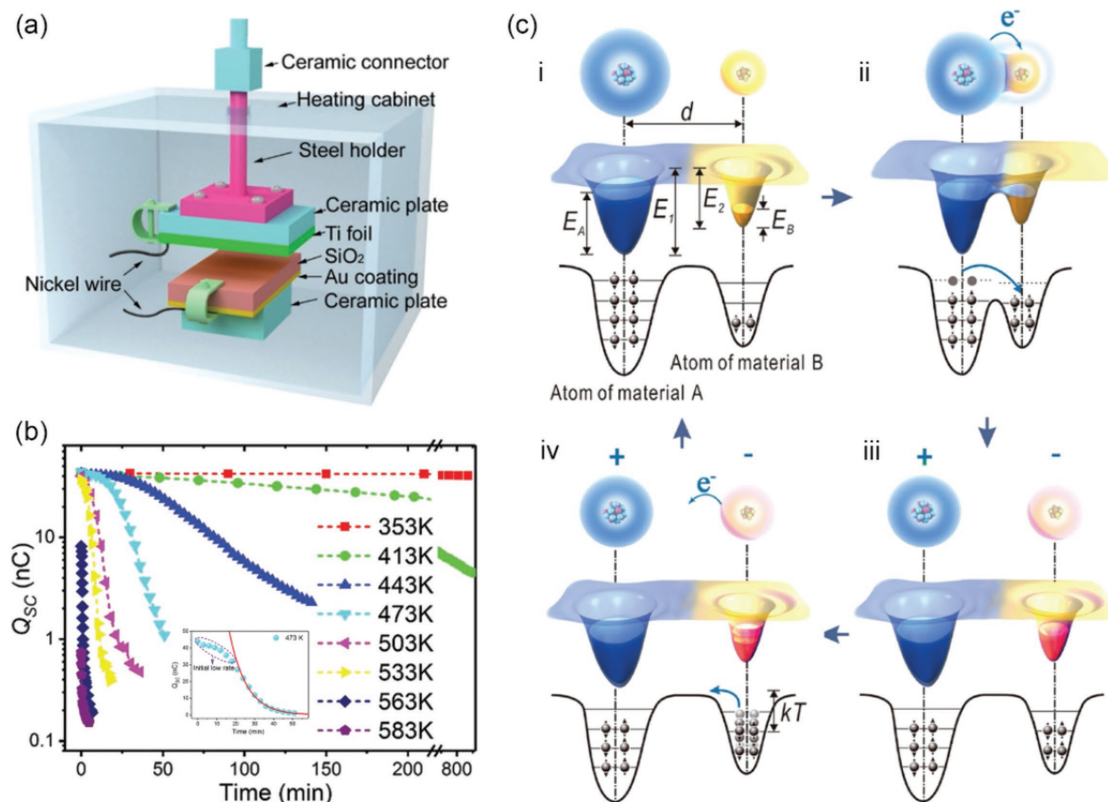MATERIALS
www.advenergymat.de

Figure 4. The electron-emission-dominated charge transfer mechanism. a) Schematic of the experimental setup for measuring the surface charge amount at high temperatures. b) Temporal evolution of measured charge transfer Q_{SC} at various temperatures. c) Proposed electron-cloud-potential-well model for the electron-transfer-dominant mechanism of contact-electrification. Reproduced with permission.[12] Copyright 2018, Wiley-VCH.

modification strategy can be further divided into chemical surface functionalization and bulk composition manipulation. In chemical surface functionalization, the triboelectric material is modified by changing the functional groups exposed on the surface so that its charge capture capability is enhanced.[47–49] For example, Wang et al. demonstrated the use of self-assembled monolayers, thiols, and silanes, to modify the surfaces of conductive material Au and dielectric material SiO_2, respectively (Figure 5a-i).[48] The results show that the output of the Au-based TENG was enhanced by the largest scale when the more triboelectrically positive function group, amine ($-NH_2$), is introduced on the Au surface, while its performance deteriorates when the triboelectrically negative group ($-Cl$) is used. The SiO_2-based TENG also receives performance improvements after silane molecules with amine as the head groups are used for surface functionalization. This surface engineering approach avoids the change in bulk material and bulk properties, and still possesses long-term stability with experimental validation after 90 d and 10k operating cycles. In bulk composition manipulation, composite materials are generally fabricated by optimizing the material composition so that the charge-attracting or charge-trapping capability is enhanced. High dielectric constant materials such as $BaTiO_3$ and $SrTiO_3$ have been widely used as fillers to enhance TENG performance,[50–52] which is also supported by theoretical studies of the dielectric effect on TENG.[53] An integrated approach by using poled ferroelectric material poly(vinylidenefluoride-co-trifluoroethylene) (P(VDF-TrFE)) as

the matrix material for charge-attracting and using embedded high-dielectric barium titanate (BTO) nanoparticles for charge-trapping, has been reported (Figure 5a-ii), achieving a 150-time boost in output power with an output voltage of 1130 V and an output current of 1.5 mA.[54] Addition of a charge transport layer such as carbon nanotubes between the triboelectric material and high dielectric material has also been proven to be effective in increasing triboelectric charge density since it facilitates the charge accumulation process.[55]

The second strategy for improving the triboelectric charge density is based on improvement of effective contact area. The effective contact area between two solid materials is generally far from 100% due to surface roughness, and thus by simply improving the contact effectiveness, the total amount of triboelectric charges will increase even if the surface charge density where the contact electrification occurs remains unchanged. One straightforward and universal approach is to introduce nano/microstructures onto the triboelectric materials, such as nanowires and pyramid/cube-like arrays (Figure 5b-i).[56,57] The second approach is the change of solid–solid friction to liquid–solid friction. Tang et al. reported the first liquid-metal-based TENG in 2015 (Figure 5b-ii) and achieved a high output charge density of 430 µC m^{-2} and an instantaneous energy conversion efficiency of up to 70.6%.[58] The liquid metal was used as both a triboelectric material and an electrode, while the other triboelectric material moved in and out of the liquid during operation. This work not only proposes a novel TENG design by utilizing
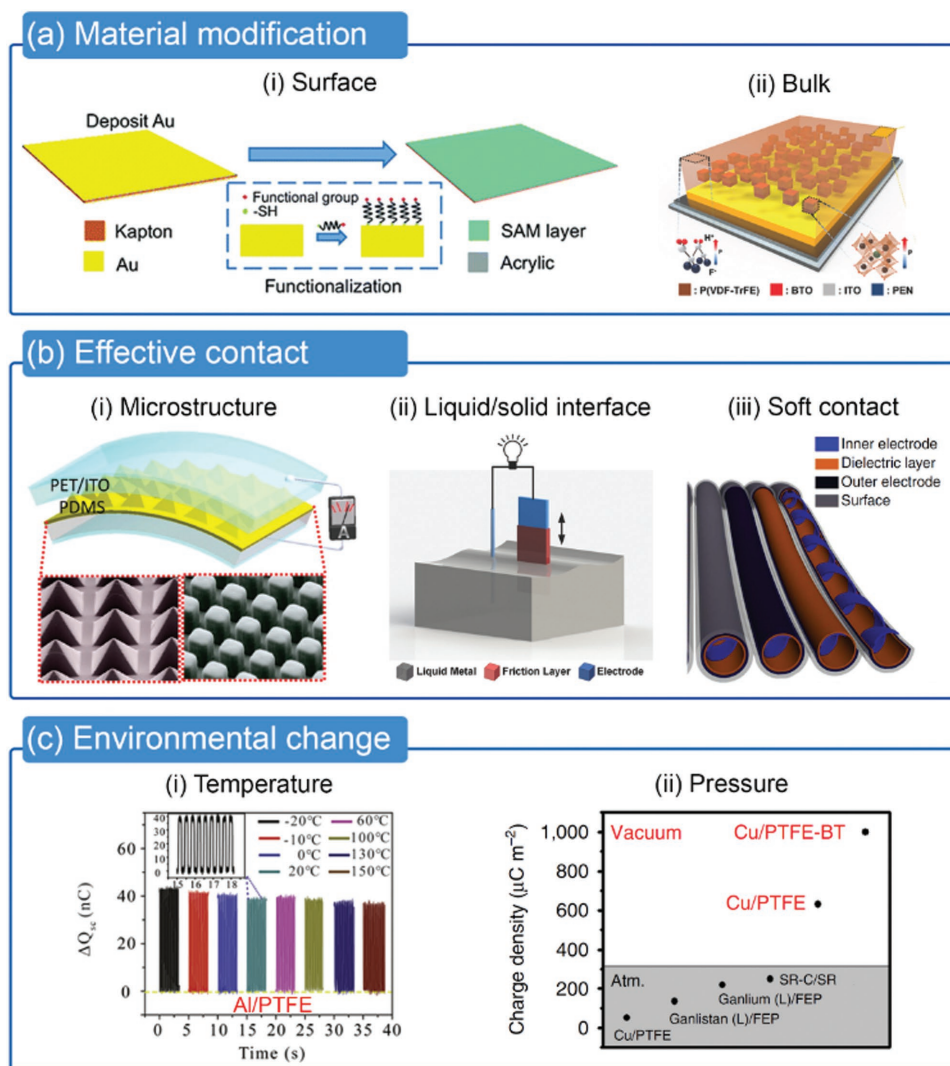
ADVANCED
SCIENCE NEWS
www.advancedsciencenews.com

ADVANCED
ENERGY
MATERIALS
www.advenergymat.de

Figure 5. Strategies for improving triboelectric charge density. a) Material modification. (i) Chemical surface functionalization. Reproduced with permission.[48] Copyright 2016, Royal Society of Chemistry. (ii) Bulk composition manipulation. Reproduced with permission.[54] Copyright 2016, Wiley-VCH. b) Improvement in effective contact area. (i) Surface microstructure. Reproduced with permission.[56] Copyright 2012, American Chemical Society. (ii) Liquid/solid interface. Reproduced with permission.[58] Copyright 2015, Wiley-VCH. (iii) Soft contact. Reproduced under the terms of the CC-BY 4.0 license.[59] Copyright 2016, Springer Nature. c) Change in environmental conditions. (i) Temperature. Reproduced with permission.[60] Copyright 2017, Wiley-VCH. (ii) Pressure. Reproduced under the terms of the CC-BY 4.0 license.[61] Copyright 2017, Springer Nature.

liquid–solid friction, but also provides an advanced tool for standardizing the triboelectric series with minimal effects from imperfect contact.[41] Moreover, soft materials such as silicone rubber tend to exhibit more intimate contact under the same applied force and thus have higher output charge density when used in TENGs. Wang et al. achieved a high charge density of 250 µC m^{-2} by fabricating a tube-like, silicone-rubber-based TENG with a rationally designed helix-belt contact structure (Figure 5b-iii).[59] Their shape-adaptive TENG can be transformed into wearable designs such as shoe soles and woven cloth, and it has been demonstrated to harvest electricity from human walking or jogging for powering wearable electronics such as an electronic watch and a fitness tracker.

The third strategy is to introduce change in environmental conditions such as temperature and pressure. Lu et al. studied

temperature effects on the performance of a PTFE-based TENG, and its electrical output decreased with temperature from −20 to 20 °C, remained relatively stable from 20 to 100 °C and dropped rapidly afterward (Figure 5c-i).[60] This temperature-dependent change in output charge density is attributed to the change in material permittivity and temperature-induced surface defects such as surface oxidation or defluorination. Another study by Xu et al. also suggests that the charge trapping capability of insulating oxides such as SiO_2 or Al_2O_3 dramatically decreases under high temperatures even though no surface defects were induced. Another environmental factor that has been well studied is air pressure.[12] Wang et al. improved the triboelectric charge density of a basic Cu-PTFE-based TENG to a record-high value of 660 µC m^{-2} by simply operating the device in high vacuum (≈10^{-6} torr), where one of

**ADVANCED
SCIENCE NEWS**
www.advancedsciencenews.com

**ADVANCED
ENERGY
MATERIALS**
www.advenergymat.de

the biggest performance-limiting factors of TENG, air break-down, was eliminated (Figure 5c-ii).[61] They further improved the record to 1003 µC m^{-2} by introducing an additional ferro-electric material (BT ceramic) layer underneath the triboelectric PTFE layer, which couples surface polarization from tribo-electrification and hysteretic dielectric polarization from the ferroelectric material. This record is close to the PTFE material limit of dielectric breakdown (≈1115 µC m^{-2}). Subsequent work by Zi et al. suggests that the use of high-voltage gases such as SF$_6$ or high-pressure gases is also effective in alleviating the air breakdown effect and improving triboelectric charge density.[62]

2.6. Power Management

Due to the randomness of ambient mechanical energy and biomechanical energy, the AC electrical outputs of TENG are usually irregular and not suitable for directly driving conventional electronics that require stable DC input power. Early solutions focused on direct integration with energy storage devices such as batteries and supercapacitors via rectifiers,[63–65] but the conversion efficiency from AC output power with high voltage and low current to stored electrochemical energy is very low due to the huge impedance mismatch between TENGs and energy storage devices. The use of conventional transformers

for reducing the voltage and boosting the current also induces huge energy loss due to the high impedance and pulsed output of TENGs.[66] Meanwhile, the output energy of TENGs is generally not maximized during standard operation cycles, with a portion of the induced charges not being transferred between electrodes.[41,67] Therefore, advanced power management methods that can achieve high energy storage efficiency are definitive and indispensable for self-powered systems, with recent progress summarized into two main strategies based on the working mechanism, that is, impedance matching via designed power converters and energy transfer maximizing via a designed charging cycle.

The first milestone in the impedance-matching-based power management of TENGs was reported by Niu et al., who developed a two-stage power management circuit.[66] Compared to the conventional circuit that connects the TENG to the energy storage unit directly through a bridge rectifier, their circuit introduces additional components including a small temporary capacitor (C_{temp}), two automatic electronic switches (J_1, J_2) with logic control units, and two coupled inductors (L_1, L_2), as shown in **Figure 6**a-i. At the first stage, the C_{temp} is charged by the TENG until it reaches the optimized charging voltage (V_{opt}), while at the second stage, the energy in C_{temp} is transferred to the final energy storage unit through the two electronic switches and the coupled inductors. More specifically, both switches J_1 and J_2 are
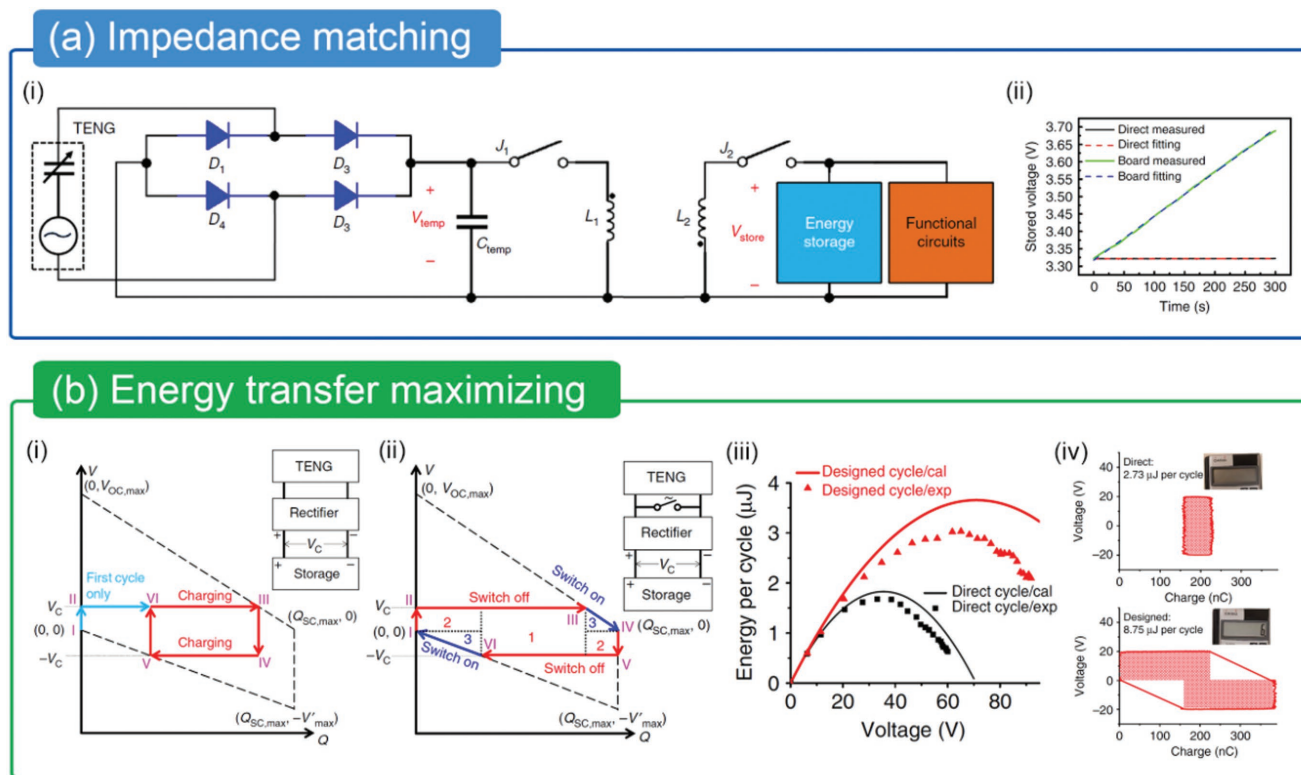

Figure 6. Power management strategies. a) Impedance matching via designed power converters. (i) Circuit diagram of impedance matching circuit. (ii) Comparison of the charging current between the direct charging and the power management board. Reproduced under the terms of the CC-BY 4.0 license.[66] Copyright 2015, Springer Nature. b) Energy transfer maximizing via designed charging cycle. (i) V–Q plot of the direct charging cycle. (ii) V–Q plot of the rationally designed charging cycle. (iii) The experimental (dots) and calculated (lines) results of the stored energy per cycle versus the charging voltage for both the direct and the designed charging cycles. (iv) Demonstration of a calculator sustainably powered with the designed charging cycle. Reproduced under the terms of the CC-BY 4.0 license.[67] Copyright 2016, Springer Nature.

ADVANCED
SCIENCE NEWS
www.advancedsciencenews.com

ADVANCED
ENERGY
MATERIALS
www.advenergymat.de

open during the first stage. When the V_{opt} is reached, J_1 closes and the energy in C_{temp} is transferred to L_1. Subsequently, J_1 opens and J_2 closes, with the energy transferred to L_2 and the final energy storage unit. By optimizing the value of C_{temp} and other electronic components, a total storage efficiency, defined as the ratio of the maximum DC power stored in an energy storage unit to the maximum AC power delivered to a resistive load, of 60% was achieved using the power management circuit, which is improved about two orders of magnitude greater than that of direct charging. The charging speed of a 1 mF capacitor using direct charging and the power management board is compared in Figure 6a-ii, which gives an improvement in charging current of over 1000 times. With integration of the power management circuit, a 15-layer TENG consisting of Kapton and FEP with dimensions of 5.7 × 5.2 × 2.4 cm yielded continuous DC electricity of 1.044 mW under palm tapping motion, and was demonstrated to sustainably drive many conventional electronics, such as a thermometer, electronic watch, calculator, and wireless car key. Subsequently, other impedance matching methods for power management using inductor-capacitor (LC) oscillators and even an inductor-free circuit, have been reported.[68,69] In the inductor-free method, a group of capacitors (N) with the same capacitance were used, and their electrical configuration was switched between series connection and parallel connection during a two-stage operation.[69] The capacitors were first charged by the TENG in a series connection, and then disconnected from the TENG and discharged to the load in a parallel connection. This conversion from series to parallel connection greatly enhanced the output charge while lowering the output voltage by a factor of N.

The other strategy of power management was proposed by Zi et al. to maximize the energy transfer out of a TENG with a rationally designed charging cycle.[67] First, the V–Q plot of a conventional direct charging cycle by connecting a SFT-mode TENG to a capacitor through a bridge rectifier, is illustrated in Figure 6b-i, with the assumption of a constant charging voltage V_C during one cycle of TENG operation. The cycle for maximized energy output with infinite load resistance is also plotted as dashed lines. In the first cycle of operation, the transferred charges Q began at 0 (state I) and started to increase when the TENG voltage reached V_C (state II). The charging stopped when the friction slider reached the maximum displacement and the Q could not reach $Q_{SC,max}$ since the output voltage V_C had to be maintained (state III). As the slider moved in the reverse direction, the charging process did not start until the output voltage of TENG reached $-V_C$ (state IV) and stopped when the slider moved back to the original position (state V). Similarly, the Q could not decrease back to 0 since $-V_C$ must be maintained. In subsequent cycles, the V–Q curves followed the sequence of V-VI-III-IV-V, with the area enclosed by red solid lines being the steady-state stored energy per cycle. It can be calculated that the maximum energy-storage efficiency, defined as the ratio of the stored energy per cycle to the maximized energy output per cycle E_m, is less than 25% after optimizing the charging voltage V_C. In the rationally designed charging cycle, a motion-triggered switch parallel to the energy storage unit was introduced, and it was turned on when the slider reached the maximum or zero displacement to allow the Q to reach $Q_{SC,max}$ and 0, respectively. Consequently, the steady-state

stored energy per cycle will have two additional parts, denoted by area 2 in Figure 6b-ii. Theoretical calculations demonstrated that maximum energy storage efficiency was improved up to 50% and the saturated charging voltage was at least twice the value of the direct charging cycle. The experimental (dots) and calculated (lines) results of the stored energy per cycle versus the charging voltage V_C for both the direct and the designed charging cycle are plotted in Figure 6b-iii, which clearly illustrates the superiority of the designed charging cycle. The demonstration in Figure 6b-iv shows that the same TENG under the same operation conditions can sustainably power the calculator with the designed charging cycle, but not with the direct one. The concept of maximizing output energy transfer by modulating the charging cycle was also realized by using an electrostatic vibrator switch[70] or an air-discharge switch,[71] with the advantage of no additional switch-control unit. An autonomous switching mechanism consisting of a micropower voltage comparator and a MOSFET was proposed as well to maximize the energy extracted from a TENG via the cycle for maximized energy output, with a maximum energy-storage efficiency of 84.6% demonstrated.[68]

The two strategies of power management can be integrated together to improve the final energy storage efficiency by maximizing the energy transfer out of TENGs and the energy conversion into energy storage units simultaneously.[68,72] Such power management circuits consist of the switch-based mechanism for achieving the cycle for maximized energy output of TENG, and the power-converter-based mechanism for impedance matching. The integrated strategy has been demonstrated to be universal for various TENGs and applications by converting ambient and human mechanical energy into sustainable and regulated electrical energy, and its development has had a profound influence on the practical application of TENG in self-powered systems.

2.7. Comparison with Electromagnetic Generator (EMG)

Among the various mechanical energy harvesting technologies, the EMG is the most widely used and has had the largest impact on human civilization. It is thus natural to compare the characteristics and performance of the emerging TENG technology with the well-established EMG, which may reveal the unique strengths and applications of TENG. The first systematic comparison work focusing on the working mechanism, governing equation, and equivalent circuit model, was reported by Zhang et al. in 2014.[73] First, they noticed that the fundamental mechanism of EMGs, electromagnetic induction, is analogous to the LS mode of TENGs. A conducting rod moves across magnetic induction lines to generate electrodynamic potential in electromagnetic induction, while a triboelectric material slides over the other to induce charge separation in the LS TENG (**Figure 7**a). The induced electrodynamic potential shares similar expression with the current flow from separated charges in the TENG mechanism, with the former depending on magnetic flux density and the latter on triboelectric charge density. When the two fundamental modes are scaled into the rotating EMG consisting of two magnets and a group of coils and the rotating TENG consisting of two segmentally patterned disks,
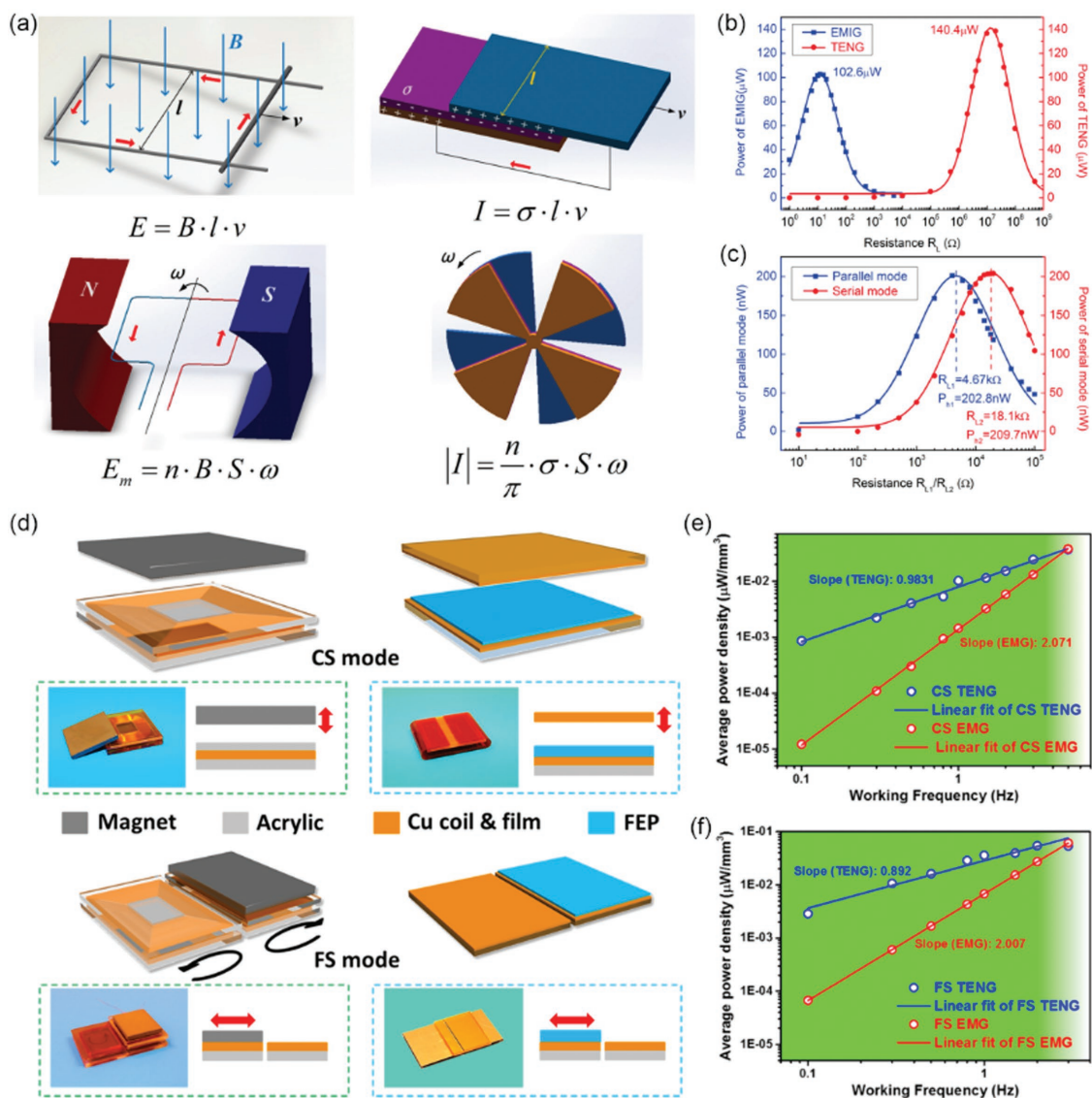
Figure 7. Comparison between EMG and TENG. a) Schematics, fundamental principles, and governing equations of the rotating EMG and TENG. b) Output power comparison of the rotating EMG and TENG. c) The conjunction operation of the rotating EMG and TENG connected in series or in parallel. Reproduced with permission.[73] Copyright 2014, Wiley-VCH. d) Schematics and photos of the CS/FS mode EMG and TENG. e,f) The average power densities of the CS mode and FS mode devices at low frequency. Reproduced with permission.[74] Copyright 2016, American Chemical Society.

respectively, their governing equations still share the same analogy. Their output power with various external load resistances were investigated as well, indicating that the TENG has a much larger matching impedance than the EMG (Figure 7b). These results suggest that from an equivalent circuit point of view, the EMG can be regarded as a voltage source with a small internal resistance while the TENG is a current source with a large internal resistance. Given that they have similar maximum output power, TENGs possess some advantages over EMGs when the device volume and weight are critical. The authors also validated that the two power sources could be transformed equivalently for the external load by connecting the EMG in series with and the TENG in parallel with a certain resistance. The conjunction operation of the two power sources connected in series or in parallel were successfully demonstrated as well,

with the maximum output power being approximately twice of that of a single EMG or TENG (Figure 7c). This work is a milestone in understanding the relationship between EMGs and TENGs, and it establishes the theoretical foundation for hybrid generators consisting of both TENGs and EMGs.

Zi et al. performed a more thorough study on comparing the low-frequency mechanical energy harvesting performance of EMG and TENG.[74] Since the CS mode and SFT mode of TENG have much higher FOM$_S$ than other modes and their analogous modes for an EMG have also been well developed for practical applications, these two modes were selected for comparison, with structures illustrated in Figure 7d. For the EMG, a magnet moved vertically on top of a set of copper coils in CS mode, while the magnet moved horizontally between two set of copper coils in SFT mode; for the TENG, a copper film moved

**ADVANCED
SCIENCE NEWS**
www.advancedsciencenews.com

**ADVANCED
ENERGY
MATERIALS**
www.advenergymat.de

vertically above a FEP film with copper coating on the back side in CS mode, while a FEP film slid between two adjacent copper films in SFT mode. Their results in Figure 7e,f show that regardless of working mode, the output power density of EMG is proportional to the square of working frequency (f^2) while that of TENG is proportional to the working frequency itself (f). This can be attributed to the fact that the open-circuit voltage of an EMG is proportional to the working frequency but that of a TENG remains constant with various frequencies. The different frequency-dependency of their outputs indicates that TENG may have better energy harvesting performance below a certain threshold frequency. Especially when it comes to powering electronic devices with a certain threshold voltage, such as LEDs, the low output voltage of EMGs at low frequency (typically 0.1–3 Hz) is inadequate while the frequency-independent output voltage of TENG (>10–100 V) is high enough to drive multiple units simultaneously. The study suggests that the TENG may find its killer applications in low-frequency mechanical energy harvesting, from small-scale biomechanical energy such as human walking to large-scale blue energy.

3. Recent Progress in TENG Applications

The major applications of TENG can be categorized into four areas: sustainable micropower sources for self-powered systems; active sensors for medical, infrastructure, environmental monitoring, and human–machine interfacing (HMI); basic networks units for harvesting low-frequency water energy toward large-scale blue energy; and direct power sources for high-voltage (HV) instruments. This section will focus on discussing the recent (2016–2018) progressions that are milestones in either revolutionizing existing directions or establishing new promising directions in these areas.

3.1. Micro/Nanoenergy Sources

Thanks to its merits such as light weight, low cost, and abundant material and structural choices, the TENG has found vast applications as micropower sources for self-powered systems by harvesting biomechanical or ambient energy, such as human walking, heartbeats, machine vibration, and wind energy. Due to its superior performance at low frequencies, biomechanical energy harvesting using TENGs is of great importance and has been explored since the very beginning phase of TENG development, with a smart backpack,[75,76] self-powered watch,[77] and acoustic energy harvester[78,79] demonstrated. Recent critical progress in this field can be categorized into two groups based on the design methodology; one is a shape-adaptive TENG for conformal power sources and the other is a fiber-based TENG for wearable power sources. It should be emphasized that these two methodologies are intertwined rather than mutually exclusive.

Shape-adaptive devices adopt elastic and deformable materials so that they can be applied on a human body in a more natural and efficient way. For example, a tube-like, silicone-based TENG that can be installed under the shoe or on clothing was developed to harvest electrical energy from human walking

for powering wearable electronics such as watches and fitness trackers.[59] Subsequently Yi et al. reported a highly stretchable TENG consisting of conductive liquid and soft rubber (**Figure 8**a).[80] The conductive liquid, such as sodium chloride solution, was encapsulated in the soft rubber, and the fabricated device could stand a tensile strain up to 300% without obvious degradation even after ≈55k deformation cycles. An optimal strain with maximum electrical outputs exists due to the conflicting effects of contact area and electrode resistance. As the strain increases, the increased contact area leads to more triboelectric charges and higher output, while the increased length and decreased cross-section area of the elongated liquid electrode induce higher resistance and lower output. This stretchable TENG could easily conform to uneven surfaces and was demonstrated as a shoe pad and wearable bracelet for harvesting energy from human walking and hand tapping. The stretchability of TENGs was further improved to a uniaxial strain of 1160% by Pu et al. using ionic conductors as the electrode.[81] The ultrastetchable, skin-like TENG (STENG) had a sandwich-like architecture with a layer of ionic hydrogel encapsulated between two elastomer films (Figure 8b). The ionic hydrogel consisted of polyacrylamide and lithium chloride, and the elastomers adopted were PDMS and VHB. Both PDMS- and VHB-STENG are highly transparent, and the stretchability and mechanical strength of the STENG could be tuned by adjusting material combination and composition. A maximum power density of 35 mW m^{-2} was achieved by using nylon to make contact-separation with the PDMS-STENG, and it was demonstrated to power an electronic watch under hand tapping. The sandwich structure greatly alleviated the dehydration of the ionic hydrogel and achieved long-term stability of the electrical outputs even after storage at a relative humidity of 30% at 30 °C for a month. Moreover, the resistance of the elongated hydrogel had much smaller increments and thus the performance degradation at stretched states was less of a concern.

Aside from in vitro energy harvesting as discussed above, a flexible and biodegradable TENG (BD-TENG) was reported by Zheng et al. for short-term in vivo biomechanical energy conversion.[82] The BD-TENG had a multilayer structure made of biodegradable polymers (BDPs) and resorbable metals (Figure 8c). It operated through the contact separation between two selected BDP layers with nanopatterned surface structures. The BDPs explored were poly(L-lactide-co-glycolide) (PLGA), poly(3-hydroxybutyric acid-co-3-hydroxyvaleric acid) (PHB/V), poly(caprolactone) (PCL), and poly(vinyl alcohol) (PVA), and magnesium thin film was deposited on the BDP layers as electrodes. The biocompatibility of these materials was validated by the viability of endotheliocytes after the cells were cultured with the BDP films for 7 d. The output voltage of the BD-TENG with a size of 2 × 3 cm could be tuned from 10 to 40 V by changing the BDP materials for triboelectrification. By changing the encapsulating BDP material from PLGA to PVA, the in vivo working durability and degradation time decreased from weeks to days. The BD-TENG was proposed to harvest energy from heartbeats, respiratory motion, and blood pressure for transient, implantable, self-powered therapeutic or diagnostic medical devices, with electric-field-assisted neuron cell orientation successfully demonstrated as an application. In addition, other functional polymers such as shape memory polymers and
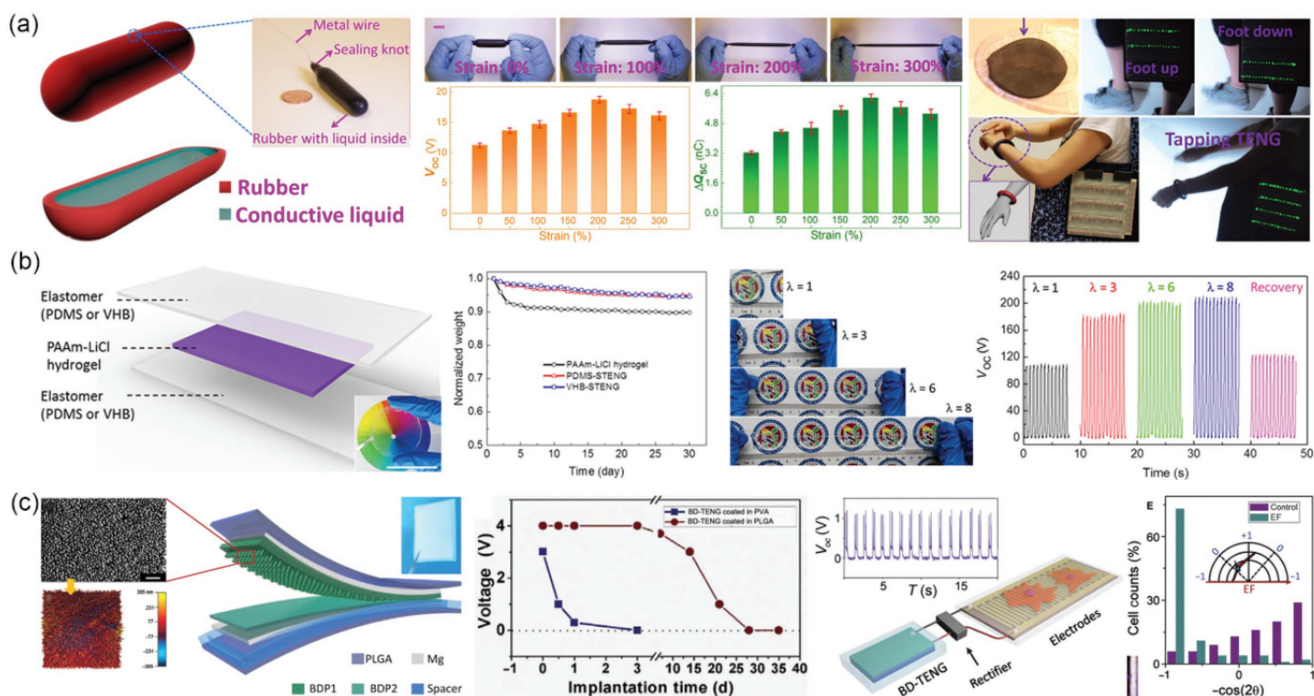
ADVANCED
SCIENCE NEWS
www.advancedsciencenews.com

ADVANCED
ENERGY
MATERIALS
www.advenergymat.de

Figure 8. Shape-adaptive TENG for conformal power sources. a) A highly stretchable TENG consisting of conductive liquid and soft rubber. Left to right: the schematic and photograph of the fabricated device; the images of the device under tensile strains and corresponding electrical outputs; demonstrations of the TENG as wearable energy harvester. Reproduced under the terms of the CC-BY-NC 4.0 license.[80] Copyright 2016, The American Association for the Advancement of Science. b) A skin-like TENG consisting of ionic hydrogel and elastomer films. Left to right: scheme of the device with a sandwich structure; comparison of dehydration rate of the hydrogel with and without encapsulation; images of a VHB-STENG at different stretched states and corresponding open-circuit voltage when having contact and separation with a latex film. Reproduced under the terms of the CC-BY-NC 4.0 license.[81] Copyright 2017, The American Association for the Advancement of Science. c) An implantable, biodegradable TENG for in vivo biomechanical energy harvesting and electrical stimulation. Left to right: device structure; electrical outputs of BD-TENGs at several time intervals after implantation; demonstration of the BD-TENG for electric-field-assisted neuron cell orientation. Reproduced under the terms of the CC-BY-NC 4.0 license.[82] Copyright 2016, The American Association for the Advancement of Science.

self-healing polymers have also been used in fabricating novel TENG devices with functional properties.[83,84]

Fiber-based power sources, such as batteries, supercapacitors, and nanogenerators, have attracted great interest in the past decade due to the emergence of wearable electronics. The first fiber-based TENG that could be woven into fabric was proposed by Zhong et al. in 2014.[85] As shown in **Figure 9**a, the fabricated device consisted of two kinds of core–shell structured fibers, with one being carbon nanotube (CNT) coated cotton threads and the other having an additional coating of PTFE on top of the CNT layer. The power generation mechanism was based on the contact separation between PTFE on one fiber and CNT on the other one, which was induced by the change in the interfiber gap when the woven cloth underwent mechanical deformation (Figure 9b). A "power shirt" made from a lab coat using the fiber-based TENGs was demonstrated to charge a commercial capacitor and trigger a wireless body temperature monitoring system (Figure 9c). 3D woven structures have been introduced to the fiber-based TENG design to improve its output performance.[86] Figure 9d shows the fabrication process of a 3D orthogonal woven TENG. The stainless-steel/polyester yarn was used to replace the CNT-coated cotton thread for easy fabrication and low cost, and PDMS was used as the other triboelectric coating. The increased number of dielectric layers in 3D woven TENG successfully improved the power outputs

when compared to single-layer woven TENG. Two types of Z-yarn for layer binding, conductive and nonconductive, were tested, and the results show that the nonconductive device had much higher electrical outputs. The proposed device design could be easily scaled to large-area wearable clothing. Furthermore, the fiber-based TENG was made to be highly stretchable by changing the core fiber material to silicone rubber,[87,88] as shown in Figure 9e. As the fiber device was stretched and released, the outer copper coil shell would be in contact (released state) and separation (stretched) with the outer silicone rubber shell, and thus the mechanical motion was converted into electrical output.

Hybrid power generation has the advantages of higher output power and harvesting various kinds of energy simultaneously. Li et al. demonstrated the concept of a fiber-based hybrid nanogenerator by integrating TENG and PENG into one single fiber with a multilayer core–shell structure.[90] Subsequently, a hybrid power textile consisting of a fabric TENG and photovoltaic (PV) textile was developed by Chen et al., with the weaving pattern and material composition illustrated in Figure 9f (Top: TENG; bottom: PV).[89] The hybrid textile could harvest solar energy and mechanical energy simultaneously, which greatly expanded its working circumstances (Figure 9g). As expected, the TENG textile generated much higher output voltage while the PV textile had much higher output current. Both the short-circuit
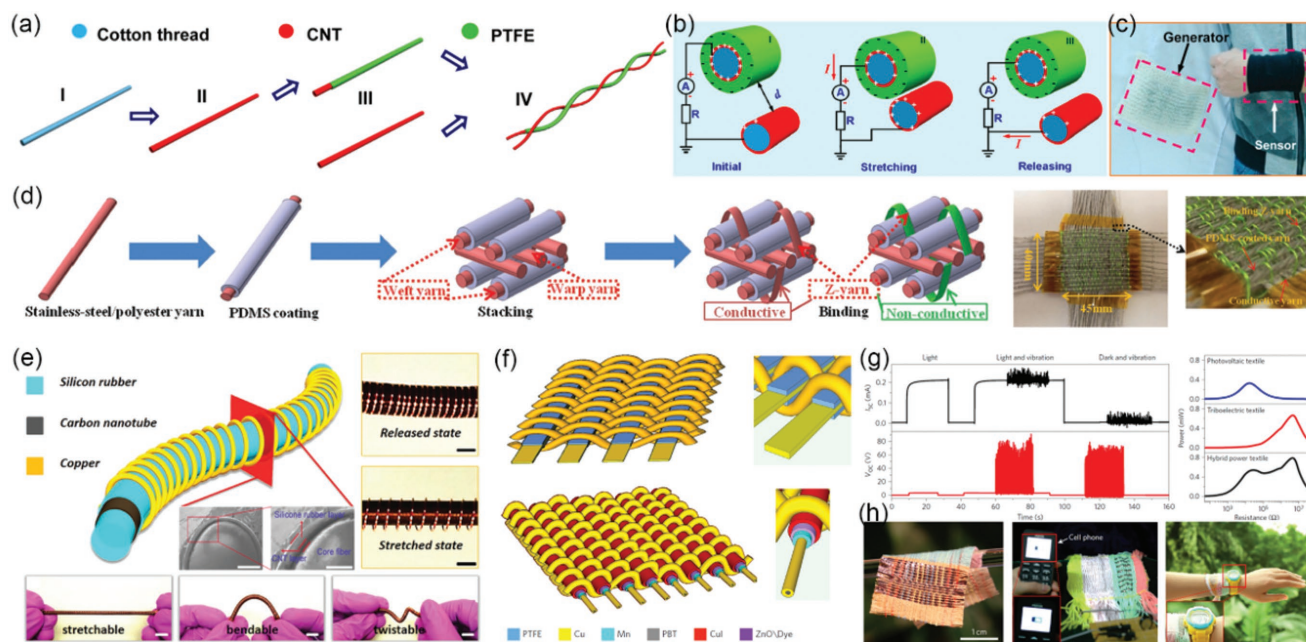
**ADVANCED
SCIENCE NEWS**
www.advancedsciencenews.com

**ADVANCED
ENERGY
MATERIALS**
www.advenergymat.de

Figure 9. Fiber-based TENG for wearable power sources. a–c) The first fiber-based TENG with its fabrication process, working mechanism, and demonstration of a "power shirt." Reproduced with permission.[85] Copyright 2014, American Chemical Society. d) The fabrication process and images of a 3D orthogonal woven TENG. Reproduced with permission.[86] Copyright 2017, Wiley-VCH. e) A stretchable fiber-based TENG using silicone rubber as the core material. Reproduced with permission.[87] Copyright 2016, Wiley-VCH. f–h) A hybrid power textile for harvesting solar and mechanical energy simultaneously. f) Structural design of fabric TENG (top) and PV textile (bottom). g) Electrical outputs of the hybrid power textile. h) Demonstration of the power textile to drive electronic devices. Reproduced with permission.[89] Copyright 2016, Springer Nature.

current and open-circuit voltage were enhanced when the two textiles functioned together. The hybridization also improved the output power over a wide range of load resistance due to huge differences in the internal impedance of the two power sources, which expanded the capability of the hybrid textile to power various electronics with different operational resistances. The hybrid textile was also demonstrated to charge a phone and an electronic watch in a wearable manner, as shown in Figure 9h. A hybridized self-charging power textile was also demonstrated by integrating fiber-shaped TENG, solar cells, and supercapacitors together.[91]

3.2. Active Sensing and Self-Powered Sensors

Since the TENG can transform mechanical stimuli to electrical signals directly without additional transducers, it has great potential in the field of active sensing and self-powered sensors, which requires less, if not zero, standby power consumption and simpler control circuits compared to traditional passive transistors. Relevant pioneering works include tactile touch sensors,[57,92,93] acoustic sensors,[78,79,94,95] motion and acceleration sensors,[96–98] and chemical sensors.[99–102] Meanwhile, with the rapid growth of the IoTs,[103,104] the development of advanced HMI has become increasingly critical to enable convenient, safe, and novel communication between humans and external devices. Given that applications of TENGs for active sensing have been reviewed comprehensively elsewhere,[29] this section will focus on discussing how the TENG-based active sensors can be used in novel HMI and transform the way people interact with machines.

Increasing concern about cyber security calls for effective and continuous authentication solutions. Keystroke dynamics, a behavioral biometric based on people's typing attributes, has the advantage of enhancing security levels without interfering with normal users' behavior.[105–107] The concept of realizing keystroke dynamics using TENG-based sensing arrays was first proposed in 2015 by Chen et al.,[108] whose device worked on the single-electrode contact separation mode and suffered from interferences of the working environment. Subsequently, based on this and other pioneering work on triboelectric keyboards,[109] we developed a two-factor, pressure-enhanced keystroke-dynamics-based security system that is capable of authenticating and even identifying users through their unique typing behavior, with an accuracy up to 98.7%.[110] The basic unit, a triboelectric key, consisted of a shield electrode and a CS-mode TENG, with silicone as the main structural material and ITO-coated PET as the electrodes (**Figure 10**a). The fabricated numeric keypad with 16 keys had the advantages of stretchability and conformality on uneven surfaces (Figure 10b). The CS-TENG transduced typing behavior into an analog electrical signal, and the adoption of a shield electrode greatly improved the signal-to-interference-plus-noise ratio from 2 to 10 dB by diminishing the effects of inadvertent touch (Figure 10c) or variations in working conditions, such as wet or dirty fingers. The designed keystroke device also introduced the effects of typing force into keystroke dynamics without additional pressure sensors, thanks to the variation in gap distance and contact area under different typing forces (Figure 10d). With the integration of a customized support-vector-machine-based software platform, keystroke features such as typing latency (L), hold time
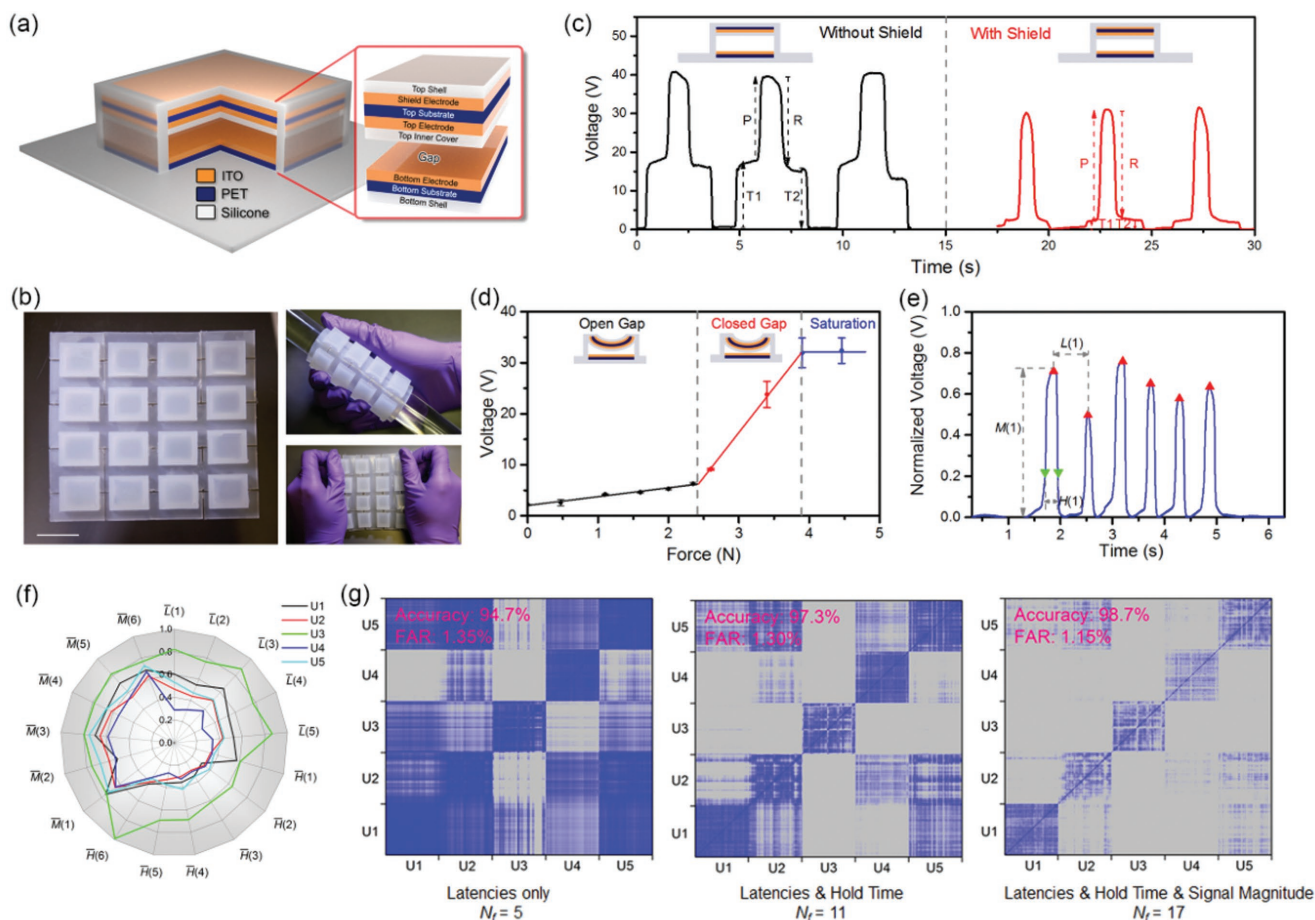
Figure 10. A keystroke-dynamics-enhanced security system using TENG array. a) Schematic and exploded view of a single triboelectric key. b) Photographs of a triboelectric numeric keypad with 16 keys (scale bar: 2 cm). c) Comparison of electrical outputs from the triboelectric key and a reference key without shield electrode. d) Relationship between the maximum output voltage and typing force. e) Typical keystroke features from typical signals for constructing user profile models. f) The radar plot of the normalized mean feature values of five users. g) The difference score matrices across user inputs with different number of features. Reproduced with permission.[110] Copyright 2018, Elsevier.

(H), and signal magnitude (M), were extracted from keystroke signals and used to construct user profile models (Figure 10e). The radar plot of the normalized mean feature values of five users after they typed the same six-digit number sequence 150 times is presented in Figure 10f and indicates distinctive typing behaviors among them. To quantify the difference between two typing inputs, the difference score matrices across user inputs are plotted in Figure 10g, with a scale ranging from 0 (gray) to 1 (blue). Ideally, the scores across the diagonal should be much lower (more blue) compared to the rest to indicate that inputs from the same user differ significantly less than those across users. The results showed more distinct typing patterns and improved system accuracy with an increase in typing features. The promising applications of this TENG-based security system in the financial and computing industry can push cyber security to the next level. This work also pioneered the development of practical active sensing applications using TENGs, rather than just proof-of-concept demonstrations. Furthermore, with the integration of optical devices such as LEDs, a SE-mode-TENG based keypad operated as a motion-triggered optical wireless transmitter and could be used to build wireless touch panels for security authentication.[111] This concept of self-powered optical

wireless transmitter using TENG-driven LEDs, which converts mechanical stimuli into optical signals directly without additional power sources, was also demonstrated for use in optical remote control and pressure sensing.[111]

Aside from applications on conventional HMI devices like keyboards, TENG-based sensors were also used to build a novel, hands-free HMI that translated real-time micromotions of eye blinking into control commands.[112] The structures and images of the proposed mechanosensational TENG (msTENG) are presented in **Figure 11**a. The single-electrode-mode msTENG had a multifilm structure, which used a tadpole-like PET film as the substrate, a FEP film and a natural latex film as the triboelectric materials, an acrylic annulus as the spacer, and ITO coated on the backside of FEP as the single electrode. It could be flexibly mounted and hidden behind an eyeglass temple via an adjustable fixator made of acrylic sheets, screws, and springs, with the natural latex touching the facial skin around the eye. During operation, the eye blinking process induces the movement of the muscle around the eye, which changes the distance between the natural latex and FEP and results in a change in the electric potential of the single electrode. By integrating the msTENG with a signal processing circuit, a smart home control
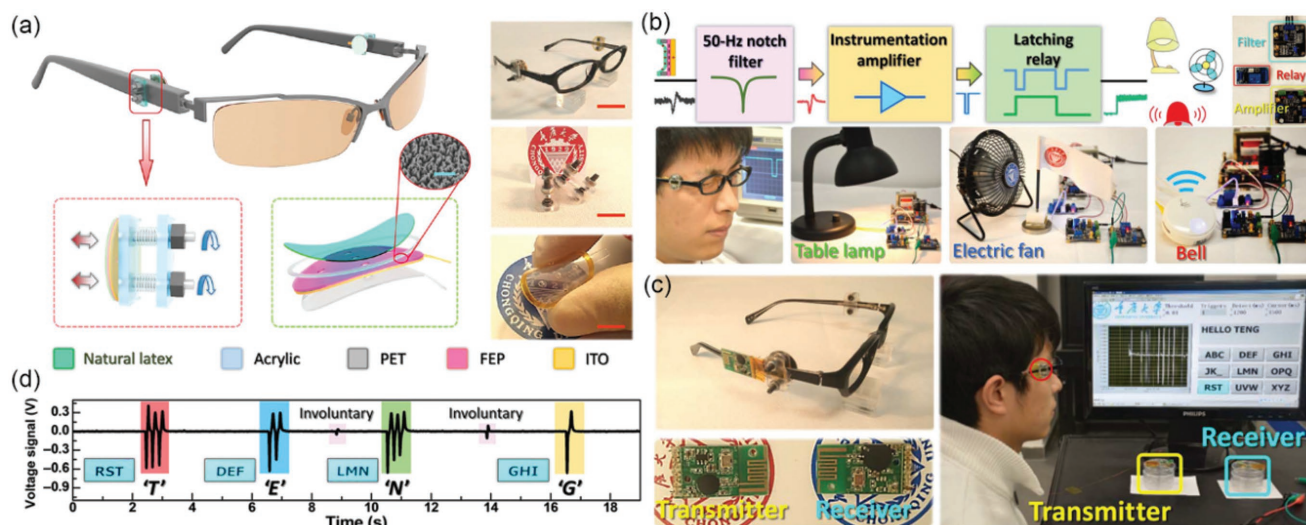
**ADVANCED
SCIENCE NEWS**

www.advancedsciencenews.com

**ADVANCED
ENERGY
MATERIALS**

www.advenergymat.de

Figure 11. Eye motion triggered mechnosensational communication system based on TENG. a) Schematic structures and photographs of the msTENG. b) A smart home control system based on the msTENG. c) A hands-free typing system based on the msTENG. d) Voltage signals from voluntarily blinking the eye when typing the word "TENG." Reproduced under the terms of the CC-BY-NC 4.0 license.[112] Copyright 2017, The American Association for the Advancement of Science.

system was developed (Figure 11b). The output signal was first filtered by a 50 Hz notch filter to eliminate power-line interference, and then amplified to drive a latching relay that connects electrical appliances and a power outlet. With the msTENG-based system, eye blinking could work like a remote prosthetic hand and control the on/off status of electrical appliances such as a table lamp, fan, and doorbell. In addition, a hands-free typing system was built by integrating the msTENG with a wireless transceiver module (Figure 11c). The user could type different letters, such as "TENG" in Figure 11d, by voluntarily blinking the eye according to the preset instructions. This non-invasive, highly sensitive TENG-based sensor enables people to control and communicate in a unique hands-free way with unprecedented convenience and intelligence.

An acoustic HMI for translating sound into electrical signals is another hands-free solution that plays an important role in information security and intelligent robotics. The first TENG-based acoustic device that could function as a sustainable energy harvester and an active sensor simultaneously was developed by Yang et al. in 2014.[78] The concept of a paper-based TENG with the same capabilities was proposed subsequently, introducing additional advantages such as ultrathinness and rollability.[79] Such devices have been demonstrated for use as an acoustic source locator and a self-powered microphone.[94,95] Recently, a self-powered triboelectric auditory sensor (TAS) was proposed for social robotics and hearing aids.[113] The multilayer TAS consisted of an Au-coated FEP film attached on an acrylic substrate, a spacer, and an Au-coated Kapton membrane (**Figure 12**a). The FEP-covered acrylic substrate had hole channels to reduce air damping and the Kapton membrane was fixed on the outer rim by an annular acrylic sheet. Membrane deformation caused by acoustic waves triggered the contact and separation between FEP and the membrane electrode, and thus generated electrical outputs. The fabricated TAS device achieved an ultrahigh sensitivity of 112.4 mV dB^{-1}, with applications

such as a sound-controllable switch and an antitheft system demonstrated. More importantly, the frequency response of the TAS could be tuned by the introduction of annular or sectional inner boundary architectures. As shown in Figure 12b, a multiresonant frequency band was achieved by a TAS with four sectorial architectures, and this feature of broadband frequency response enables it to have applications in an electronic auditory system with high quality and fidelity in sound recording. Therefore, it can also be used in security systems using voice recognition. As in Figure 12c, the electrical signals from two different persons saying the same word "Hello" were recorded by the TAS device, and the results of power spectral density estimation (PSDE) and joint time-frequency analysis (JTFA) showed distinctive differences between the users. Moreover, the TAS has huge potential in hearing aids since the signals of the impaired frequency region can be naturally enhanced through device design. Figure 12d shows the sound waves and corresponding acoustic spectrograms of original voices, weakened voices (−30 dB in the 207–837 and 1594–2090 Hz frequency regions) played by a loudspeaker, and recorded voices by a TAS-based hearing aid system, which clearly indicates the sound information in the impaired frequency regions was restored. Such a TAS-based system greatly reduces the complexity and cost of signal processing circuits in conventional hearing aids.

3.3. Blue Energy

The application of TENGs in harvesting natural mechanical energy, such as wind energy,[114–117] raindrop energy,[118–120] ultrasonic energy,[121] and water wave energy,[122–124] has attracted numerous research interests. Among them, the concept of using a TENG to harvest the kinetic energy of water waves in the vast oceans, that is, blue energy,[15,125] is particularly important, since recent studies suggest that a TENG is
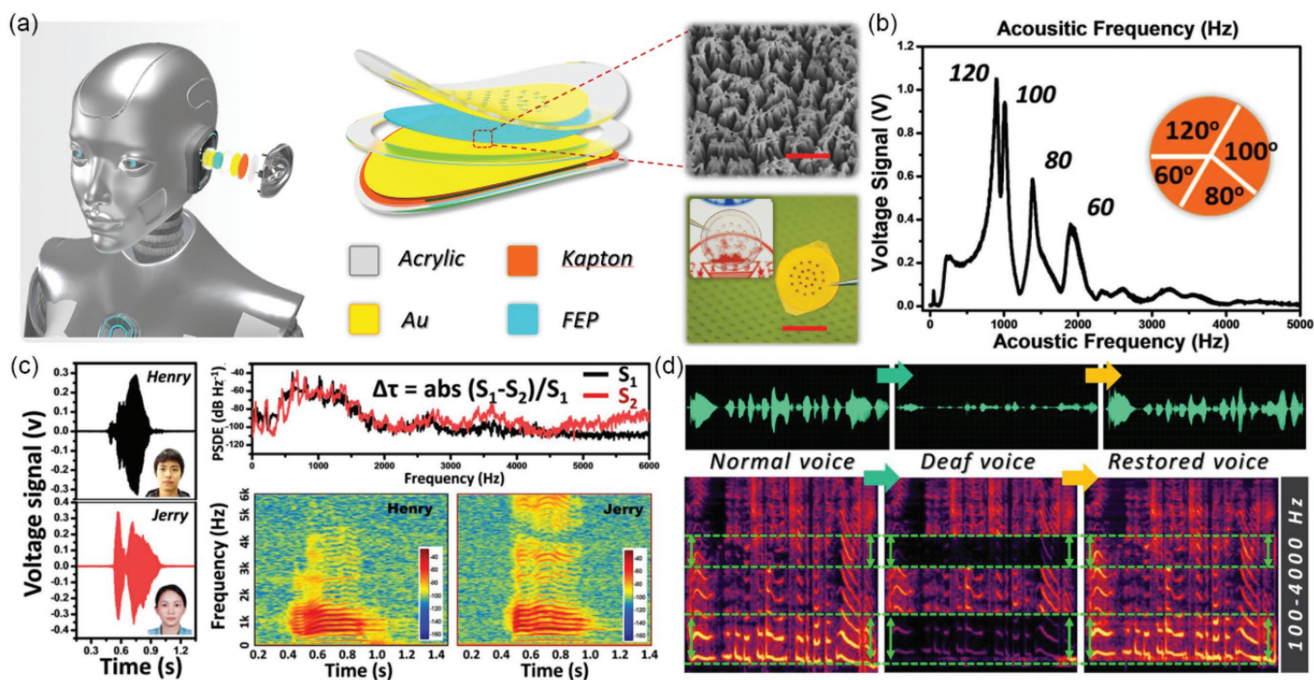
Figure 12. A triboelectric auditory sensor for social robots and hearing aids. a) Schematics and photographs of the TAS. b) Broadband frequency response of the TAS with four sectorial boundaries. c) Security application of the TAS in voice recognition. d) Medical application of the TAS in hearing aids for restoring impaired frequency region. Reproduced with permission.[113] Copyright 2018, The American Association for the Advancement of Science.

more effective than an EMG when it comes to harvesting low-frequency (<5 Hz) vibration energy.[74]

Among the various forms of TENGs proposed for blue energy, such as vertical plates with parallel electrodes[126,127] and arch-shaped TENG walls enclosing a rolling ball,[128] the fully enclosed rolling spherical structure is regarded as the most promising since it can harvest the energy from all directions.[129] **Figure 13**a presents a typical rolling-structured, freestanding-triboelectric-layer-mode TENG (RF-TENG) enclosed in a spherical shell for blue energy harvesting, which lit up 70 green LEDs while stimulated by a wave generator. The RF-TENG consisted of a rolling Nylon ball and a Kapton film with two stationary back electrodes attached to the inner surface of the spherical shell. Its operating principle is illustrated in Figure 13b. The rolling of the freestanding Nylon ball on the Kapton film generated opposite charges on their surfaces (state i), and as the ball rolled from the left to the right, the electric potential of the two electrodes changed, inducing an output voltage and current when connected to the external circuit (state ii). This process continued until the ball reached the top of the right electrode (iii). As the ball moved backward, an opposite current flow was induced until it reached the left electrode again. Consequently, the kinetic energy of water waves inducing the relative motion between the ball and the shell was converted to AC electrical outputs. At a wave frequency of 1.43 Hz, the RF-TENG could achieve a short-circuit charge transfer of about 24 nC cycle^{-1} and an open-circuit voltage up to 12 kV (Figure 13c). The dependency of output on the wave frequency was investigated as well, showing a uniform and significant response characteristic within the frequency range of 1.23–1.55 Hz (Figure 13d). The results indicated that

the natural frequency of the RF-TENG was within the low-frequency range of water waves (typically <2 Hz) and thus it is suitable for efficient blue energy harvesting. The performance of the rolling spherical design was further improved by the optimization of materials. As shown in Figure 13e, soft silicone rubber was used to fabricate the ball and the dielectric layer on the shell so that the effective area for triboelectrification was increased due to more intimate contact.[130] UV treatment of the silicone ball and mixture of polyformaldehyde (POM) particles into the silicone dielectric layer greatly enhanced the output performance, as indicated by the comparison study in Figure 13f. To harvest the blue energy in a large scale, the concept of using coupled TENG networks was proposed by Wang et al., and optimal connection mechanisms among the TENG units have always been a crucial subject worth investigation. Three different types of connection as shown in Figure 13g, that is, rigid plate connection which will not deform, elastic strip connection that can deform to some extent, and string connection that can freely deform without extension, have been proposed and studied. The results in Figure 13h show that flexible connections by either the string or an elastic strip of a 4 × 4 network exhibited much better performance (current and transferred charge) than rigid ones, which can be attributed to the redundant internal constraints between units in the latter strategy. As a demonstration, a thermometer was powered by the string-connected network to measure water temperature (Figure 13i).

Spring-based structures capable of converting instantaneous impact energy into elastic potential energy for extra operation cycles can further improve the efficiency of TENG in low-frequency energy harvesting. As shown in **Figure 14**a,
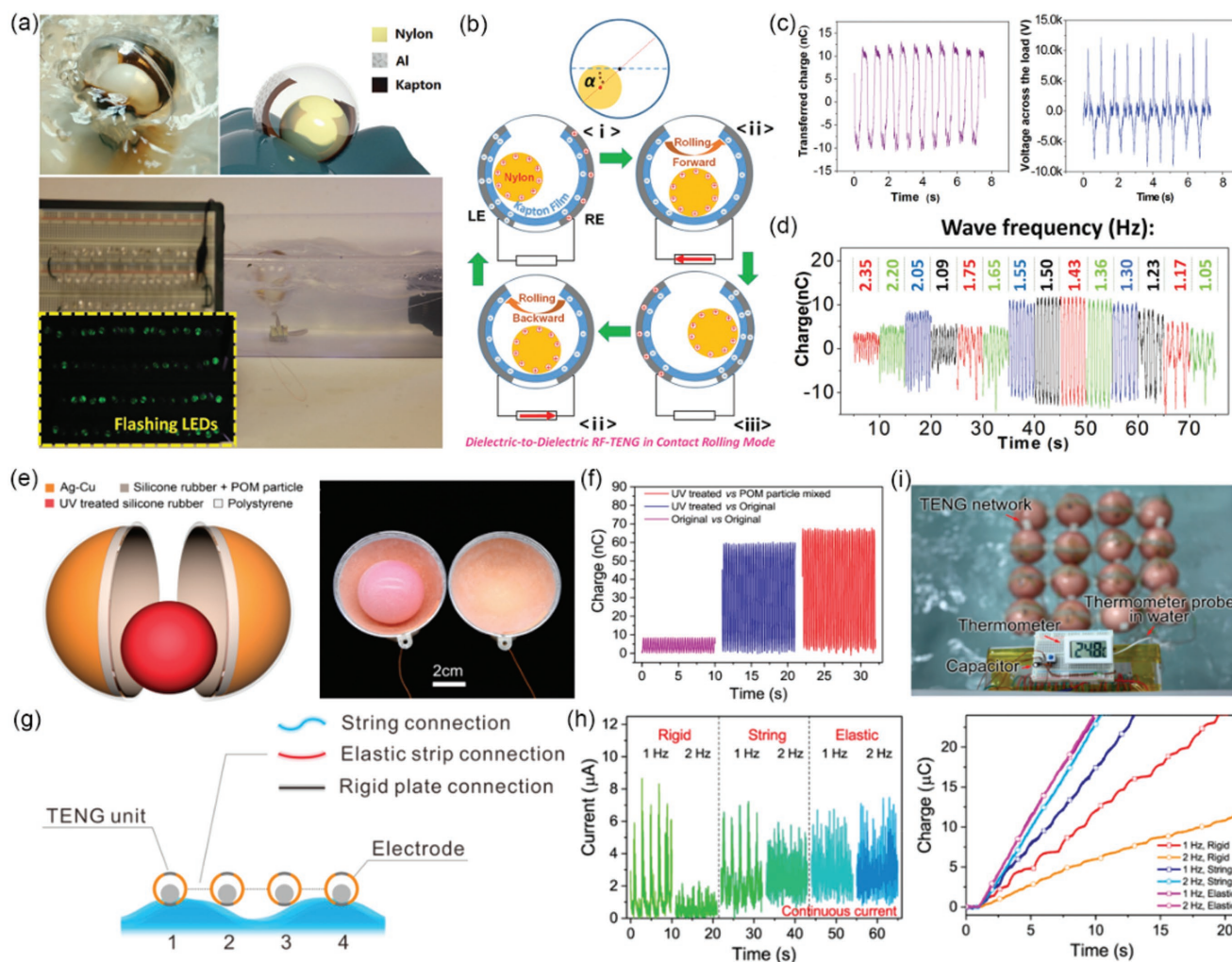
Figure 13. Ball-shell structured blue energy harvester using TENG. a–d) RF-TENG. a) Photographs and schematic, b) working principle, c) typical electrical outputs at a wave frequency of 1.43 Hz, and d) dependency of output on the wave frequency of the RF-TENG. Reproduced with permission.[129] Copyright 2015, Wiley-VCH. e–i) Coupled TENG network. e) Schematic and photograph of silicone-based ball-shell TENG. f) Comparison of output performance by modifying the silicone material. g) Schematic of different types of connection among TENG units. h) Comparison of output performance between different connections. i) Demonstration of a string-connected TENG network to power a thermometer. Reproduced with permission.[130] Copyright 2018, American Chemical Society.

a type of spring-assisted TENG for blue energy harvesting was proposed by Jiang et al.,[131] which consisted of an acrylic box and two spring-connected acrylic blocks. Cu electrodes were anchored on the two internal walls of the box and Cu-coated PTFE films were attached on the block surfaces, resulting in contact and separation between PTFE and Cu under external mechanical vibration. When triggered by a linear motor, the typical electrical outputs of the spring-assisted TENG and a reference TENG using an acrylic strip to connect the two blocks are compared in Figure 14b. The accumulated charge per cycle was improved from 351.03 to 747.84 nC, and many more current peaks were observed from the spring-assisted TENG. This is explained by the fact that the connection spring can store part of the impact energy as elastic potential energy, and then release it to induce more cycles of TENG operation. Consequently, the energy output per cycle was improved by 150% when using the spring. Multiples of such units were

integrated in a single external box to improve the output current of a single device, which greatly enhanced its capability to drive electronic devices such as LEDs (Figure 14c,d). Furthermore, a type of mechanical amplifier consisting of coupled springs has been proven to be effective in enhancing the performance of a single-spring resonator based TENG (SR-TENG).[132] The schematics of a mechanical amplifier-assisted TENG (MA-TENG) and a SR-TENG are presented in Figure 14e. Both operated on the SE mode with Cu and PTFE as the triboelectric materials, and the key difference was the split of one weight (m_0) into two weights (m_1 and m_2) connected by a spring. Theoretical study of collisions in the two kinds of devices suggested that the sequential collisions between the bottom base, m_1, and m_2 in the MA-TENG enabled m_2 to gain a higher upward velocity than m_0, which made the PTFE film contact the top Cu electrode more easily and more frequently (Figure 14f). The current outputs of the two devices under the same 6 Hz
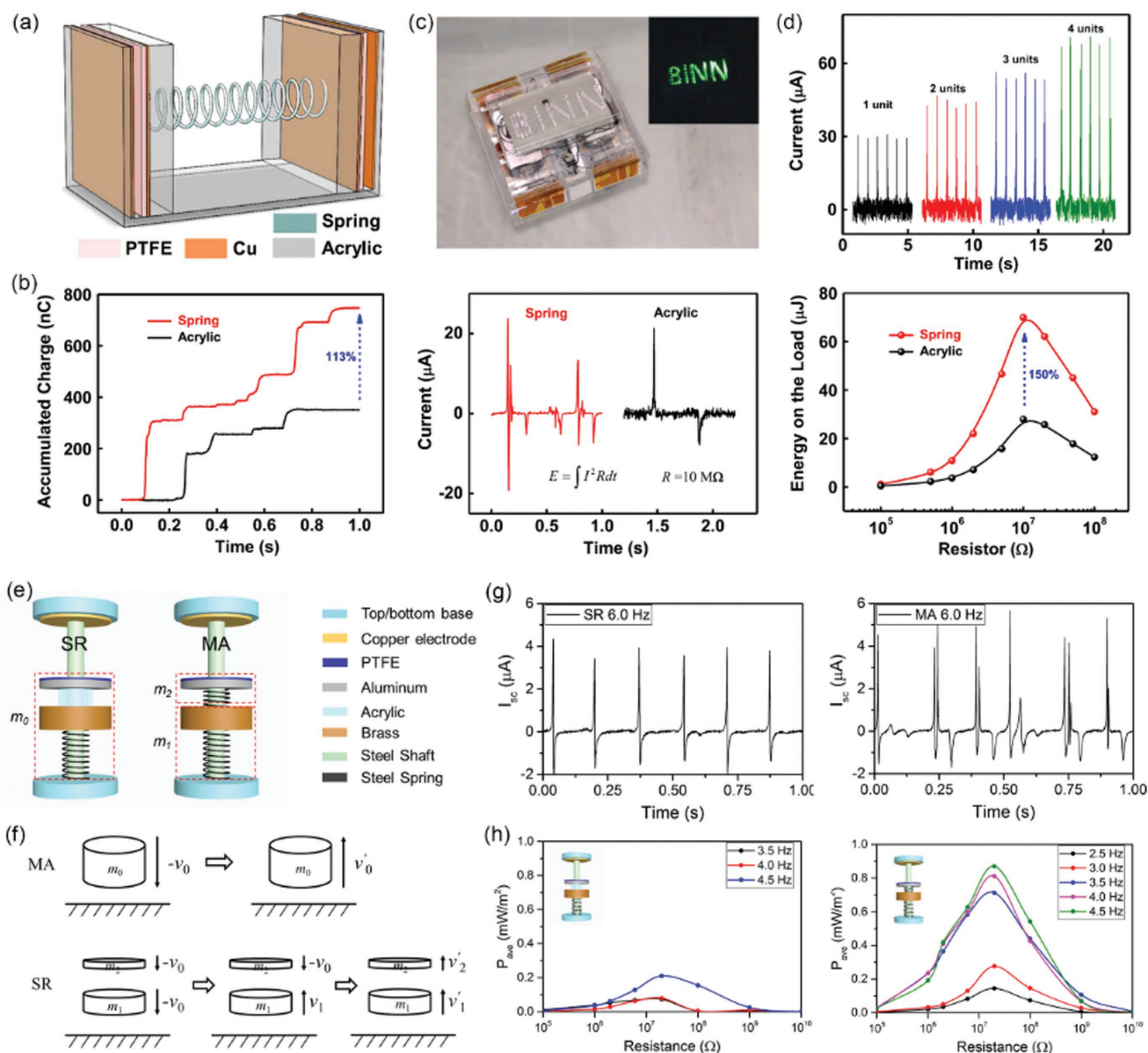
ADVANCED
SCIENCE NEWS
www.advancedsciencenews.com

ADVANCED
ENERGY
MATERIALS
www.advenergymat.de

Figure 14. Spring-based structures for improving TENG efficiency in harvesting low-frequency energy. a–d) A spring-assisted TENG device for blue energy harvesting. a) Schematic of the structure. b) Comparison of electrical outputs between the spring-assisted TENG and a reference TENG with an acrylic-strip connection. c) Photograph of an enclosed device consisting of four units. d) Comparison of the output current with respect to the number of units in a device. Reproduced with permission.[131] Copyright 2017, Elsevier. e–h) Spring-based resonance coupling for enhancing TENG performance. e) Schematics of the SR- and MA-TENG. f) Schematic of sequential collisions in the two TENGs. g) Comparison of output current at 6.0 Hz vibration. h) Comparison of average output power at various vibration frequencies. Reproduced with permission.[132] Copyright 2017, Elsevier.

vibration frequency clearly validated the higher output frequency from the MA-TENG (Figure 14g). By comparing their average output power under various frequencies between 2.5 and 4.5 Hz, it was obvious that MA-TENG had enhanced performance under low-frequency vibration, achieving a maximum power ratio of 10:1 at 4.0 Hz (Figure 14h). These works demonstrate the great potential of improvement in TENG performance and its promising prospect in large-scale blue energy.

Alternatively, by using strings of sphere TENGs that are arranged row by row, it is possible to harvest wind energy,

especially from mild wind. This can be a major complement to conventional wind power generators that only operate under severe wind conditions.

3.4. Direct HV Power Sources

The intrinsic characteristics of high voltage and low current render the TENG as a novel alternative of conventional HV power sources with unprecedented portability and safety. With an easily

ADVANCED
SCIENCE NEWS
www.advancedsciencenews.com

ADVANCED
ENERGY
MATERIALS
www.advenergymat.de

obtainable high voltage of 1–10 kV, the TENG-based HV sources usually do not require sophisticated power converters, which greatly reduces the system complexity and cost. Given the limited charge transfer per operation cycle, the ideal HV application of TENG should have little requirements on current so that comparable, if not better, performance can be achieved when compared to conventional sources. Also, the lower current poses much less threat to the safety of personnel and instruments since HV could not be maintained once the limited charge is transferred.

One excellent example in this field is the use of TENG to generate nanoelectrospray ionization for highly sensitive nano-coulomb molecular mass spectrometry (MS),[133] which not only utilizes the HV output of TENG, but also transforms the limitation of charge transfer into an advantage of unprecedented control over ion generation. As shown in **Figure 15**a, a discrete amount of pulsed charges from the SF TENG were supplied to a nano electrospray ionization (nanoESI) emitter and triggered highly repeatable ionization pulses with
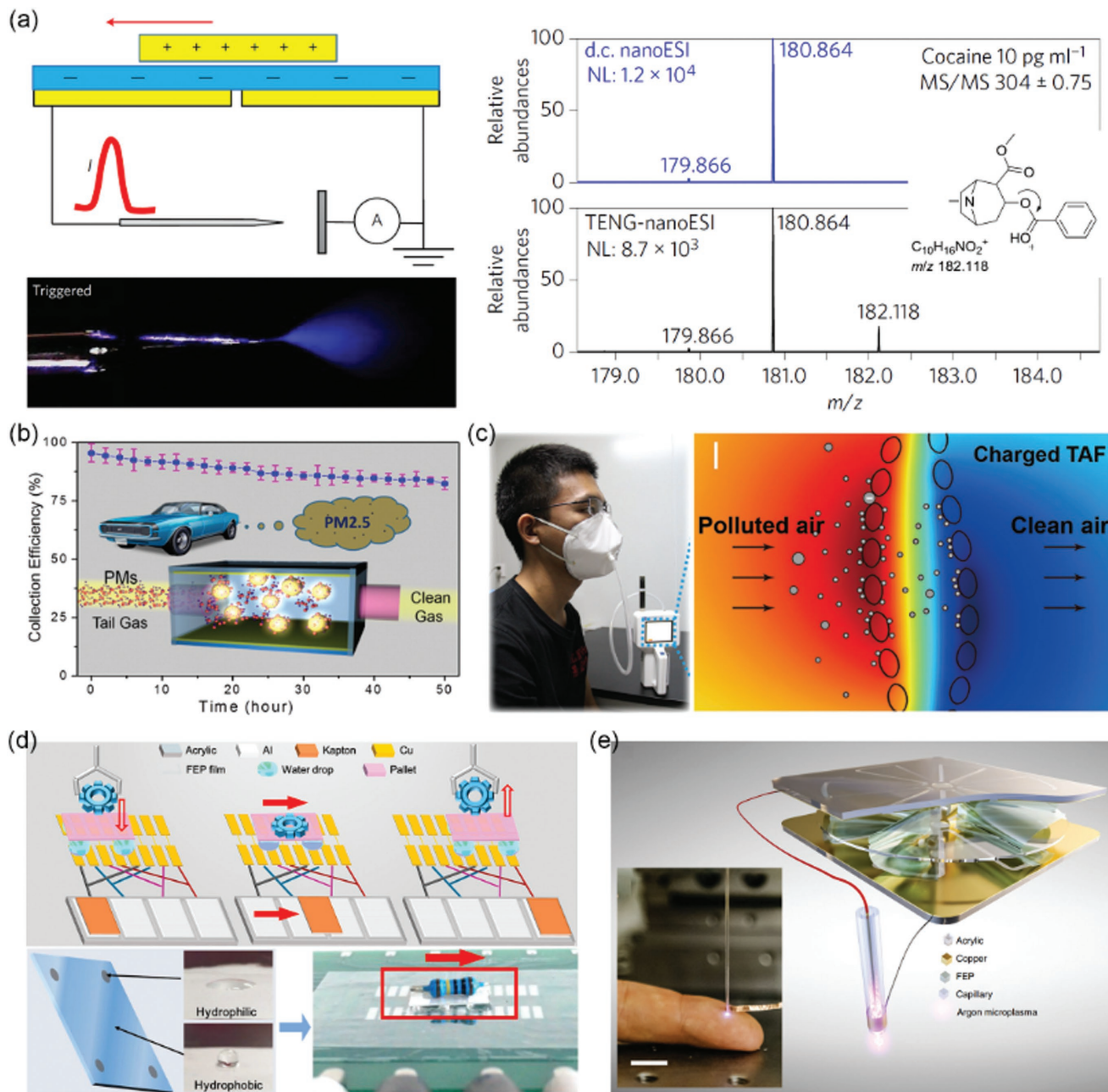

Figure 15. Application of TENG as direct HV power sources. a) Sensitive nano-coulumb molecular mass spectrometry. Reproduced with permission.[133] Copyright 2017, Springer Nature. b) PM removal from automobile exhaust fumes. Reproduced with permission.[134] Copyright 2015, American Chemical Society. c) Washable air filter. Reproduced with permission.[22] Copyright 2018, Wiley-VCH. d) Microfluidic transport system. Reproduced with permission.[135] Copyright 2018, American Chemical Society. e) Triboelectric microplasma. Reproduced under the terms of the CC-BY 4.0 license.[136] Copyright 2018, Springer Nature.

**ADVANCED
SCIENCE NEWS**
www.advancedsciencenews.com

**ADVANCED
ENERGY
MATERIALS**
www.advenergymat.de

minimum sample consumption. The duration, frequency, and ion polarity were all tunable via TENG actuation on-demand, and the high voltage (5–9 kV) of the TENG provided nanoESI with enhanced sensitivity at low concentrations, as demonstrated by the signature fragment ion (m/z 182.118) only observable in the SF-TENG-driven nanoESI MS when analyzing a cocaine solution (10 pg mL^{-1}).

TENG-driven air cleaning, which was first proposed by Chen et al. in 2014,[21] is based on electrostatic precipitation and has huge potential in commercialization with the growing severity of air pollution. Compared to conventional electrostatic precipitators, it can be self-powered and have no concern about ozone generation. The concept was first demonstrated using a wind-driven rotating TENG, whose rectified DC output was supplied to two parallel electrodes.[21] Charged particles were then collected by the electrodes due to Coulombic forces of attraction and repulsion. It was also demonstrated that the particulate matter (PM) removal efficiency of conventional fibrous filters could be enhanced using a rotating TENG.[137] Moreover, a self-powered triboelectric filter consisting of vibratory PTFE pellets and electrode plates was developed to remove the PM in automobile exhaust fumes using the self-vibration of the tailpipe, achieving a mass collection efficiency of ≈95.5% for PM$_{2.5}$ (Figure 15b).[134] Recently, a washable multiplayer triboelectric air filter (TAF) consisting of nylon fabrics and PTFE fabrics was developed.[22] The TAF could be charged by simply rubbing the fabrics against each other and achieved a removal efficiency of 84.7 and 96.0% for PM$_{0.5}$ and PM$_{2.5}$, respectively. Unlike commercial face masks, the removal efficiency was barely changed after the TAF was cleaned with commercial detergent, which makes it highly promising in fabricating a reusable and efficient face mask (Figure 15c).

The high voltage of TENGs can also be used for electrostatic actuation. Chen et al. demonstrated a TENG-driven actuation system based on dielectric elastomer actuators, which could modulate the on/off status of an intelligent switch or the spacing of tunable optical gratings.[138,139] With rationally designed electrodes on a chosen substrate, the voltage output of TENG provided the Coulomb force that modulated the motion of tiny objects such as water droplets and solid pellets.[140] As shown in Figure 15d, a self-powered microfluidic transport system driven by TENG was developed based on the working mechanism.[135] A mini vehicle consisting of four water droplets and an object-carrying pallet was placed on a hydrophobic surface, under which two lines of grating track Cu-electrodes were placed to guide the motion of the droplets. The track electrodes were connected periodically to the grid electrodes of a FS TENG, which consisted of a movable Kapton film and four pieces of Al foil attached on an acrylic plate. As the Kapton moved, the output voltage of TENG generated Coulomb force to move the droplets and thus the mini vehicle.

With the integration of voltage boosting circuits, the voltage of a TENG can reach above 10 kV and can be used to drive many other HV processes such as electrospinning,[141] electron field emission,[142] and microplasma.[136] Recently, the concept of triboelectric microplasma was realized by Cheng et al. via the integration of TENG with a plasma source, and atmospheric-pressure plasma powered only by mechanical stimuli was achieved (Figure 15e). Application of the triboelectric microplasma for surface treatment and patterned luminescence was demonstrated successfully, and the work is believed to enrich the diversity of plasma applications beyond the reach of existing technologies by offering a facile and portable supplement to traditional plasma sources. With the advantages of portability, controllability, safety, and high efficiency, TENG-based power sources are believed to have wide applications in many fields, such as HV instruments, actuators, environmental protection, and human health.

4. Summary and Perspectives

Ever since the invention of electromagnetic induction in 1831 by Faraday, the electromagnetic generator has been the driving mechanical energy harvester that powers the world. The EMG is most efficient for converting high-frequency, regular, and high-quality energy into electric power. Since the output current of EMG is conduction current, the output voltage of an EMG is its current multiplied by the load resistance. Since the inner resistance of an EMG is the resistance of the metal coils, the match resistance for an EMG is usually low, thus, its output voltage is low. In contrast, TENG is dominated by the displacement current and its output current is a capacitive conduction current; the output voltage is fixed regardless of operation frequency. In such a case, it is easy to achieve good operation voltage even at rather low frequencies. In regards to slow and random energy dispersed in our living environment, TENGs are most effective for converting such energy into useful output power, which is what we need in the era of IoTs.

Ever since the discovery of the TENG in 2012, its rapid development has quickly excited many research communities from energy to sensors. It is being studied across 40 countries, over 400 units and by over 3000 scientists. In summary from current research, the TENG is likely to impact four major fields across many disciplines. First, it is a micro/nanopower source for small and mobile electronics simply because of its performance and the ever present availability of mechanical agitations. The TENG can be integrated with existing sensor devices for building a self-powered system; each can work independently and be distributed in environment, but all of them can form a network for real-time, in situ sensing in any area of interest, such as mapping water quality/pollution, forest fire prevention, human population distribution, and animal tracking. Second, it can serve as an active sensor that is self-powered for sensing any mechanical motion and agitation in the field of HMI, robotics, artificial intelligence, and security. Once we can build self-powered sensors, their significance would be analogous to the revolution from wired communication to wireless communication. Third, in cases where we can fully integrate many units of TENGs into a network and their performance is improved by using different materials and design, it is possible to build a large-scale energy harvesting system using the energy offered by water waves and wind, which is referred as the blue energy. Finally, the TENG can be a high-voltage source for specific HV applications, such as exciting plasma, field emission, and more.

Based on the above summarized four fields, a road map for TENG is proposed, as presented in **Figure 16**, which identifies
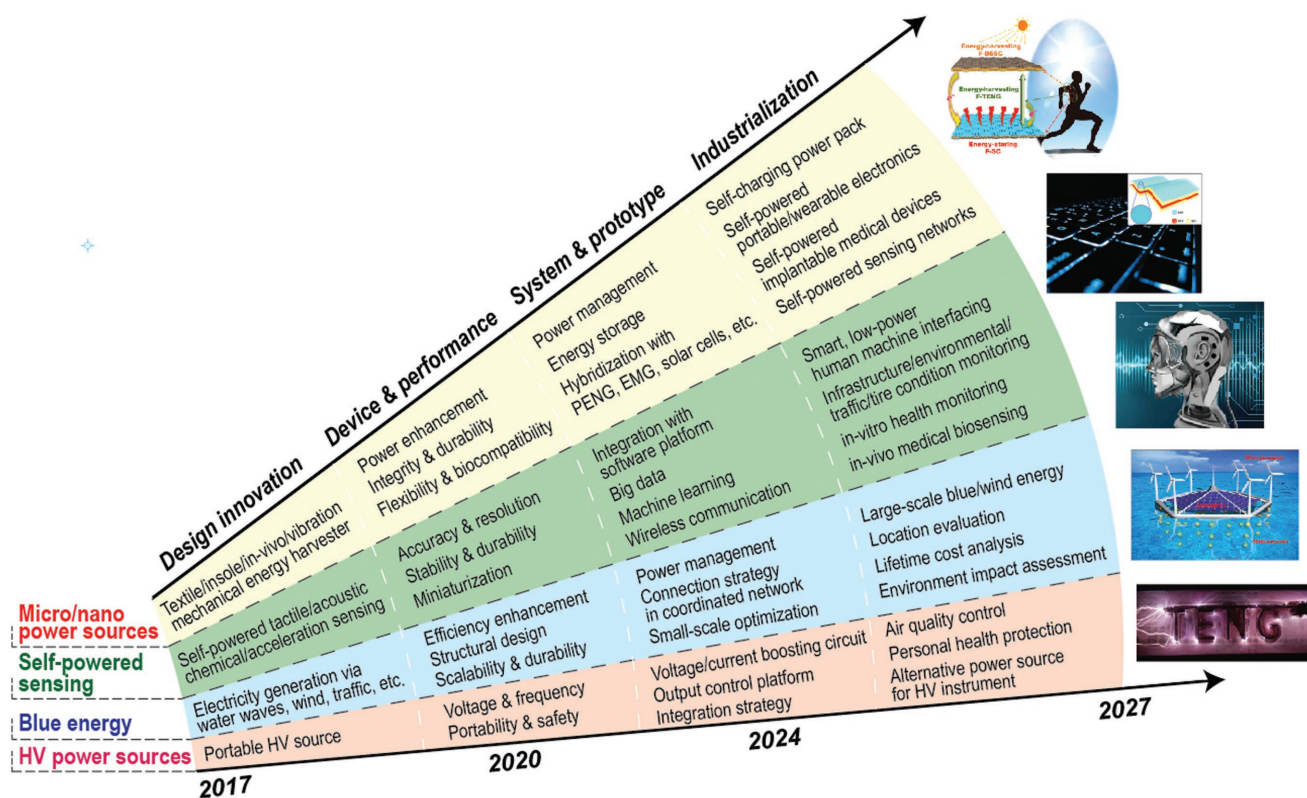
ADVANCED
SCIENCE NEWS

www.advancedsciencenews.com

ADVANCED
ENERGY
MATERIALS

www.advenergymat.de

Figure 16. Road map of TENG development from 2017 to 2027. Reproduced under the terms of the CC-BY-NC 4.0 license.[91] Copyright 2016, The American Association for the Advancement of Science. Reproduced with permission.[108] Copyright 2015, American Chemical Society. Reproduced with permission.[15] Copyright 2017, Elsevier. Reproduced under the terms of the CC-BY 4.0 license.[136] Copyright 2018, Springer Nature.

key priority directions and key challenges for TENG. Each field is likely to experience four stages, but the pace at which each stage proceeds may vary from field to field. First, design innovation is required in order to design the best TENG structure for the specific purposes of conjoining the four working modes. Second, for the specific design, the most suitable materials are chosen for achieving the maximized performance with consideration of the working environment and durability. Third, system integration, prototype testing, and product development are essential and possibly will take longer for TENG to reach commercialization. Finally, an industry based on TENGs and related technologies is anticipated for its vast applications and across many fields.

In order to achieve such high goals, Z. L. Wang summarized the ten questions related to TENG in 2014.[3] Some of the questions have been answered by now, and here are listed a few that remain to be addressed.

1. Fundamental physics of triboelectrification. Although we have made some progress in understanding triboelectrification, plenty more work remains to explore triboelectrification at nanoscale by controlling the atmosphere and temperature. Such studies are in progress by using atomic force microscopy and Kelvin probe microscopy. More importantly, theoretical research and related calculations starting from the first principle are required to understand triboelectrification, a room temperature and even high temperature quantum transition process. This is a new field for physicists.

2. High-performance triboelectric materials that exhibit the highest surface charge density. The output power is proportional to the square of the surface charge density. The electrostatic induction in TENG is also related to the dielectric constant of the materials. Both key parameters have to be improved for achieving the maximized performance. This is possible by creating proper surface micro/nanostructures not only for enhancing surface area but also for creating the effective contacts. The other suggestion is the use of composite materials. This is a promising research topic for materials people.

3. Durability of the materials and devices. One of the key concerns regarding triboelectrification is the durability of the surface structure. We do not expect a major decay in contact-separation mode TENGs, but for sliding mode TENGs it could be a problem. Two possible solutions are suggested. The first one is developing materials that have the most robust mechanical durability and stability possible by using composite structures. The second one is using a conjunction of working modes for the TENG.[143] Once the triboelectric charges are on surfaces, they remain there for hours and even days without dissipation. This means that the mechanical contacts are required only for the first few cycles (<10 cycles) and the remaining cycles of operation do not require direct contact of the two surfaces until perhaps after a few hours later, while the output power is not expected to be significantly affected. In such a case, no heat, no debris and

ADVANCED
SCIENCE NEWS

www.advancedsciencenews.com

ADVANCED
ENERGY
MATERIALS

www.advenergymat.de

friction would exist or be generated! The lifetime of a TENG could be effectively extended. Therefore, we need to design such mechanical "switchable" structures that allow for an occasional contact of the two surfaces without affecting operation. This is an innovative challenge for mechanical engineers.

4. The operation of TENG sensitively depends on moisture and atmosphere. We previously found that the surface charge density can be improved by a factor of 5 once it is operated in vacuum.[61] Therefore, good packaging materials are required for water prevention and sealing. This should be addressed by chemists and materials scientists.

5. The operation temperature of TENGs can be from as low as liquid nitrogen temperature to as high as ≈400 °C owing to electron thermion emission in triboelectrification.[13] Further raising of the working temperature above which the tribo-electrification is still preserved is a new challenge, but an exciting problem for materials scientists.

6. Energy storage. The current existing research focuses on charging a battery or supercapacitor using a DC input. However, for TENGs, the input power for the energy storage unit is a pulsed input. The dynamics introduced by the pulse drive for Li ion transport has to be considered with regard to the thickness of the separation film in the Li battery, in order to ensure effective transport of Li ions to the counter electrode.[144] Second, the leakage problem for supercapacitors has to be addressed for TENG energy storage at low current.[145] These are new problems for people who are working in the field of energy storage.

7. System integration. As for blue energy, it is vitally important to study the behavior of TENGs in fluids, especially with the introduction of springs for enhancing the energy harvested efficiency. The network behavior and the structure design and optimization have to be considered in a real water working environment. In such areas, we need not only expertise in fluid and mechanical engineering, but also network design from an electronics point of view regarding power management and system integration.

8. Environmental interaction. In the case of using TENG strings or networks for harvesting wind energy, studying their aerodynamics is needed in order to maximize their output.

These critical problems, along with the directions identified in the road map, suggest vast opportunities in TENG development for researchers and entrepreneurs across broad fields. It is anticipated that the TENG field will continue its rapid growth in the next decade and some killer applications of TENG will start to play an important role in commercial markets, possibly forming a TENG dominated enterprise. We truly believe that time will test our proposed road map and verify our predictions.

Acknowledgements

Conflict of Interest

The authors declare no conflict of interest.

Keywords

[1] F. A. Furfari, *IEEE Ind. Appl. Mag.* **2005**, *11*, 10.
[2] F.-R. Fan, Z.-Q. Tian, Z. L. Wang, *Nano Energy* **2012**, *1*, 328.
[3] Z. L. Wang, *Faraday Discuss.* **2014**, *176*, 447.
[4] S. Wang, L. Lin, Z. L. Wang, *Nano Lett.* **2012**, *12*, 6339.
[5] S. Wang, L. Lin, Y. Xie, Q. Jing, S. Niu, Z. L. Wang, *Nano Lett.* **2013**, *13*, 2226.
[6] G. Zhu, J. Chen, Y. Liu, P. Bai, Y. S. Zhou, Q. Jing, C. Pan, Z. L. Wang, *Nano Lett.* **2013**, *13*, 2282.
[7] Y. Yang, H. Zhang, J. Chen, Q. Jing, Y. S. Zhou, X. Wen, Z. L. Wang, *ACS Nano* **2013**, *7*, 7342.
[8] S. Wang, Y. Xie, S. Niu, L. Lin, Z. L. Wang, *Adv. Mater.* **2014**, *26*, 2818.
[9] Z. L. Wang, *ACS Nano* **2013**, *7*, 9533.
[10] Z. L. Wang, J. Chen, L. Lin, *Energy Environ. Sci.* **2015**, *8*, 2250.
[11] A. C. Wang, C. Wu, D. Pisignano, Z. L. Wang, L. Persano, *J. Appl. Polym. Sci.* **2018**, *135*, 45674.
[12] C. Xu, Y. Zi, A. C. Wang, H. Zou, Y. Dai, X. He, P. Wang, Y.-C. Wang, P. Feng, D. Li, Z. L. Wang, *Adv. Mater.* **2018**, *30*, 1706790.
[13] C. Xu, A. C. Wang, H. Zou, B. Zhang, C. Zhang, Y. Zi, L. Pan, P. Wang, P. Feng, Z. Lin, Z. L. Wang, *Adv. Mater.* **2018**, *30*, 1803968.
[14] G. Zhu, Y. S. Zhou, P. Bai, X. S. Meng, Q. Jing, J. Chen, Z. L. Wang, *Adv. Mater.* **2014**, *26*, 3788.
[15] Z. L. Wang, T. Jiang, L. Xu, *Nano Energy* **2017**, *39*, 9.
[16] H. Askari, A. Khajepour, M. B. Khamesee, Z. Saadatnia, Z. L. Wang, *Nano Today* **2018**.
[17] M. Li, A. L. Porter, Z. L. Wang, *Nano Energy* **2017**, *34*, 93.
[18] H. Peng, X. Fang, S. Ranaei, Z. Wen, A. L. Porter, *Nano Energy* **2017**, *35*, 358.
[19] A. Ahmed, I. Hassan, T. Ibn-Mohammed, H. Mostafa, I. M. Reaney, L. S. C. Koh, J. Zu, Z. L. Wang, *Energy Environ. Sci.* **2017**, *10*, 653.
[20] B. Wang, Y. Liu, Y. Zhou, Z. Wen, *Nano Energy* **2018**, *46*, 322.
[21] S. Chen, C. Gao, W. Tang, H. Zhu, Y. Han, Q. Jiang, T. Li, X. Cao, Z. Wang, *Nano Energy* **2015**, *14*, 217.
[22] Y. Bai, C. B. Han, C. He, G. Q. Gu, J. H. Nie, J. J. Shao, T. X. Xiao, C. R. Deng, Z. L. Wang, *Adv. Funct. Mater.* **2018**, *28*, 1706680.
[23] S. Niu, Z. L. Wang, *Nano Energy* **2015**, *14*, 161.
[24] Y. Zi, Z. L. Wang, *APL Mater.* **2017**, *5*, 074103.
[25] R. Hinchet, W. Seung, S.-W. Kim, *ChemSusChem* **2015**, *8*, 2327.
[26] F. R. Fan, W. Tang, Z. L. Wang, *Adv. Mater.* **2016**, *28*, 4283.
[27] S. Rathore, S. Sharma, B. P. Swain, R. Kr. Ghadai, *IOP Conf. Ser.: Mater. Sci. Eng.* **2018**, *377*, 012186.
[28] Y. Wang, Y. Yang, Z. L. Wang, *NPJ Flexible Electron.* **2017**, *1*, 10.
[29] S. Wang, L. Lin, Z. L. Wang, *Nano Energy* **2015**, *11*, 436.
[30] J. Chen, Z. L. Wang, *Joule* **2017**, *1*, 480.
[31] Z. Wen, J. Fu, L. Han, Y. Liu, M. Peng, L. Zheng, Y. Zhu, X. Sun, Y. Zi, *J. Mater. Chem. C* **2018**.

[32] Z. L. Wang, *Mater. Today* **2017**, *20*, 74.

[33] S. Niu, S. Wang, L. Lin, Y. Liu, Y. S. Zhou, Y. Hu, Z. L. Wang, *Energy Environ. Sci.* **2013**, *6*, 3576.

[34] S. Niu, Y. Liu, S. Wang, L. Lin, Y. S. Zhou, Y. Hu, Z. L. Wang, *Adv. Mater.* **2013**, *25*, 6184.

[35] S. Niu, S. Wang, Y. Liu, Y. S. Zhou, L. Lin, Y. Hu, K. C. Pradel, Z. L. Wang, *Energy Environ. Sci.* **2014**, *7*, 2339.

[36] S. Niu, Y. Liu, X. Chen, S. Wang, Y. S. Zhou, L. Lin, Y. Xie, Z. L. Wang, *Nano Energy* **2015**, *12*, 760.

[37] S. Niu, Y. Liu, Y. S. Zhou, S. Wang, L. Lin, Z. L. Wang, *IEEE Trans. Electron Devices* **2015**, *62*, 641.

[38] T. Jiang, X. Chen, C. B. Han, W. Tang, Z. L. Wang, *Adv. Funct. Mater.* **2015**, *25*, 2928.

[39] R. D. I. G. Dharmasena, J. H. B. Deane, S. R. P. Silva, *Adv. Energy Mater.* **2018**, 1802190.

[40] R. D. I. G. Dharmasena, K. D. G. I. Jayawardena, C. A. Mills, J. H. B. Deane, J. V. Anguita, R. A. Dorey, S. R. P. Silva, *Energy Environ. Sci.* **2017**, *10*, 1801.

[41] Y. Zi, S. Niu, J. Wang, Z. Wen, W. Tang, Z. L. Wang, *Nat. Commun.* **2015**, *6*, 8376.

[42] J. Lowell, *J. Phys. D: Appl. Phys.* **1977**, *10*, 65.

[43] C.-Y. Liu, A. J. Bard, *Chem. Phys. Lett.* **2009**, *480*, 145.

[44] H. A. Mizes, E. M. Conwell, D. P. Salamida, *Appl. Phys. Lett.* **1990**, *56*, 1597.

[45] H. T. Baytekin, A. Z. Patashinski, M. Branicki, S. Baytekin, S. Soh, B. A. Grzybowski, *Science* **2011**, *333*, 308.

[46] W. R. Harper, *Contact and Frictional Electrification*, Clarendon, Oxford **1967**.

[47] W.-C. Lin, S.-H. Lee, M. Karakachian, B.-Y. Yu, Y.-Y. Chen, Y.-C. Lin, C.-H. Kuo, J.-J. Shyue, *Phys. Chem. Chem. Phys.* **2009**, *11*, 6199.

[48] S. Wang, Y. Zi, Y. S. Zhou, S. Li, F. Fan, L. Lin, Z. L. Wang, *J. Mater. Chem. A* **2016**, *4*, 3728.

[49] S. Wang, Y. Xie, S. Niu, L. Lin, C. Liu, Y. S. Zhou, Z. L. Wang, *Adv. Mater.* **2014**, *26*, 6720.

[50] X. Chen, K. Parida, J. Wang, J. Xiong, M.-F. Lin, J. Shao, P. S. Lee, *ACS Appl. Mater. Interfaces* **2017**, *9*, 42200.

[51] A. Danish, Y. Bin, D. Xiaochao, Y. Hao, Z. Meifang, *Nanotechnology* **2017**, *28*, 075203.

[52] J. Chen, H. Guo, X. He, G. Liu, Y. Xi, H. Shi, C. Hu, *ACS Appl. Mater. Interfaces* **2016**, *8*, 736.

[53] S. Kim, J. Ha, J.-B. Kim, *Integr. Ferroelectr.* **2016**, *176*, 283.

[54] W. Seung, H.-J. Yoon, T. Y. Kim, H. Ryu, J. Kim, J.-H. Lee, J. H. Lee, S. Kim, Y. K. Park, Y. J. Park, S.-W. Kim, *Adv. Energy Mater.* **2017**, *7*, 1600988.

[55] N. Cui, L. Gu, Y. Lei, J. Liu, Y. Qin, X. Ma, Y. Hao, Z. L. Wang, *ACS Nano* **2016**, *10*, 6131.

[56] F.-R. Fan, L. Lin, G. Zhu, W. Wu, R. Zhang, Z. L. Wang, *Nano Lett.* **2012**, *12*, 3109.

[57] L. Lin, Y. Xie, S. Wang, W. Wu, S. Niu, X. Wen, Z. L. Wang, *ACS Nano* **2013**, *7*, 8266.

[58] W. Tang, T. Jiang, F. R. Fan, A. F. Yu, C. Zhang, X. Cao, Z. L. Wang, *Adv. Funct. Mater.* **2015**, *25*, 3718.

[59] J. Wang, S. Li, F. Yi, Y. Zi, J. Lin, X. Wang, Y. Xu, Z. L. Wang, *Nat. Commun.* **2016**, *7*, 12744.

[60] C. X. Lu, C. B. Han, G. Q. Gu, J. Chen, Z. W. Yang, T. Jiang, C. He, Z. L. Wang, *Adv. Eng. Mater.* **2017**, *19*, 1700275.

[61] J. Wang, C. Wu, Y. Dai, Z. Zhao, A. Wang, T. Zhang, Z. L. Wang, *Nat. Commun.* **2017**, *8*, 88.

[62] Y. Zi, C. Wu, W. Ding, Z. L. Wang, *Adv. Funct. Mater.* **2017**, *27*, 1700049.

[63] S. Wang, Z.-H. Lin, S. Niu, L. Lin, Y. Xie, K. C. Pradel, Z. L. Wang, *ACS Nano* **2013**, *7*, 11263.

[64] J. Wang, X. Li, Y. Zi, S. Wang, Z. Li, L. Zheng, F. Yi, S. Li, Z. L. Wang, *Adv. Mater.* **2015**, *27*, 4830.

[65] Q. Jiang, C. Wu, Z. Wang, A. C. Wang, J.-H. He, Z. L. Wang, H. N. Alshareef, *Nano Energy* **2018**, *45*, 266.

[66] S. Niu, X. Wang, F. Yi, Y. S. Zhou, Z. L. Wang, *Nat. Commun.* **2015**, *6*, 8975.

[67] Y. Zi, J. Wang, S. Wang, S. Li, Z. Wen, H. Guo, Z. L. Wang, *Nat. Commun.* **2016**, *7*, 10987.

[68] F. Xi, Y. Pang, W. Li, T. Jiang, L. Zhang, T. Guo, G. Liu, C. Zhang, Z. L. Wang, *Nano Energy* **2017**, *37*, 168.

[69] Y. Zi, H. Guo, J. Wang, Z. Wen, S. Li, C. Hu, Z. L. Wang, *Nano Energy* **2017**, *31*, 302.

[70] J. Yang, F. Yang, L. Zhao, W. Shang, H. Qin, S. Wang, X. Jiang, G. Cheng, Z. Du, *Nano Energy* **2018**, *46*, 220.

[71] G. Cheng, H. Zheng, F. Yang, L. Zhao, M. Zheng, J. Yang, H. Qin, Z. Du, Z. L. Wang, *Nano Energy* **2018**, *44*, 208.

[72] X. Cheng, L. Miao, Y. Song, Z. Su, H. Chen, X. Chen, J. Zhang, H. Zhang, *Nano Energy* **2017**, *38*, 438.

[73] C. Zhang, W. Tang, C. Han, F. Fan, Z. L. Wang, *Adv. Mater.* **2014**, *26*, 3580.

[74] Y. Zi, H. Guo, Z. Wen, M.-H. Yeh, C. Hu, Z. L. Wang, *ACS Nano* **2016**, *10*, 4797.

[75] W. Yang, J. Chen, G. Zhu, J. Yang, P. Bai, Y. Su, Q. Jing, X. Cao, Z. L. Wang, *ACS Nano* **2013**, *7*, 11317.

[76] A. Chandrasekhar, N. R. Alluri, V. Vivekananthan, Y. Purusothaman, S.-J. Kim, *J. Mater. Chem. C* **2017**, *5*, 1488.

[77] T. Quan, X. Wang, Z. L. Wang, Y. Yang, *ACS Nano* **2015**, *9*, 12301.

[78] J. Yang, J. Chen, Y. Liu, W. Yang, Y. Su, Z. L. Wang, *ACS Nano* **2014**, *8*, 2649.

[79] X. Fan, J. Chen, J. Yang, P. Bai, Z. Li, Z. L. Wang, *ACS Nano* **2015**, *9*, 4236.

[80] F. Yi, X. Wang, S. Niu, S. Li, Y. Yin, K. Dai, G. Zhang, L. Lin, Z. Wen, H. Guo, J. Wang, M.-H. Yeh, Y. Zi, Q. Liao, Z. You, Y. Zhang, Z. L. Wang, *Sci. Adv.* **2016**, *2*, e1501624.

[81] X. Pu, M. Liu, X. Chen, J. Sun, C. Du, Y. Zhang, J. Zhai, W. Hu, Z. L. Wang, *Sci. Adv.* **2017**, *3*, e1700015.

[82] Q. Zheng, Y. Zou, Y. Zhang, Z. Liu, B. Shi, X. Wang, Y. Jin, H. Ouyang, Z. Li, Z. L. Wang, *Sci. Adv.* **2016**, *2*, e1501478.

[83] R. Liu, X. Kuang, J. Deng, Y.-C. Wang, A. C. Wang, W. Ding, Y.-C. Lai, J. Chen, P. Wang, Z. Lin, H. J. Qi, B. Sun, Z. L. Wang, *Adv. Mater.* **2018**, *30*, 1705195.

[84] J. Deng, X. Kuang, R. Liu, W. Ding, A. C. Wang, Y.-C. Lai, K. Dong, Z. Wen, Y. Wang, L. Wang, H. J. Qi, T. Zhang, Z. L. Wang, *Adv. Mater.* **2018**, *30*, 1705918.

[85] J. Zhong, Y. Zhang, Q. Zhong, Q. Hu, B. Hu, Z. L. Wang, J. Zhou, *ACS Nano* **2014**, *8*, 6273.

[86] K. Dong, J. Deng, Y. Zi, Y.-C. Wang, C. Xu, H. Zou, W. Ding, Y. Dai, B. Gu, B. Sun, Z. L. Wang, *Adv. Mater.* **2017**, *29*, 1702648.

[87] X. He, Y. Zi, H. Guo, H. Zheng, Y. Xi, C. Wu, J. Wang, W. Zhang, C. Lu, Z. L. Wang, *Adv. Funct. Mater.* **2017**, *27*, 1604378.

[88] J. Park, A. Y. Choi, C. J. Lee, D. Kim, Y. T. Kim, *RSC Adv.* **2017**, *7*, 54829.

[89] J. Chen, Y. Huang, N. Zhang, H. Zou, R. Liu, C. Tao, X. Fan, Z. L. Wang, *Nat. Energy* **2016**, *1*, 16138.

[90] X. Li, Z.-H. Lin, G. Cheng, X. Wen, Y. Liu, S. Niu, Z. L. Wang, *ACS Nano* **2014**, *8*, 10674.

[91] Z. Wen, M.-H. Yeh, H. Guo, J. Wang, Y. Zi, W. Xu, J. Deng, L. Zhu, X. Wang, C. Hu, L. Zhu, X. Sun, Z. L. Wang, *Sci. Adv.* **2016**, *2*, e1600097.

[92] Y. Yang, H. Zhang, Z.-H. Lin, Y. S. Zhou, Q. Jing, Y. Su, J. Yang, J. Chen, C. Hu, Z. L. Wang, *ACS Nano* **2013**, *7*, 9213.

[93] G. Zhu, W. Q. Yang, T. Zhang, Q. Jing, J. Chen, Y. S. Zhou, P. Bai, Z. L. Wang, *Nano Lett.* **2014**, *14*, 3208.

[94] A. Yu, M. Song, Y. Zhang, Y. Zhang, L. Chen, J. Zhai, Z. Wang, *Nano Res.* **2015**, *8*, 765.

ADVANCED
Science News

www.advancedsciencenews.com

ADVANCED
ENERGY
MATERIALS

www.advenergymat.de

[95] N. Arora, S. L. Zhang, F. Shahmiri, D. Osorio, Y.-C. Wang, M. Gupta, Z. Wang, T. Starner, Z. L. Wang, G. D. Abowd, *Proc. ACM Interact., Mobile, Wearable Ubiquitous Technol.* **2018**, *2*, 1.

[96] Y. S. Zhou, G. Zhu, S. Niu, Y. Liu, P. Bai, Q. Jing, Z. L. Wang, *Adv. Mater.* **2014**, *26*, 1719.

[97] F. Yi, L. Lin, S. Niu, J. Yang, W. Wu, S. Wang, Q. Liao, Y. Zhang, Z. L. Wang, *Adv. Funct. Mater.* **2014**, *24*, 7488.

[98] C. Wu, X. Wang, L. Lin, H. Guo, Z. L. Wang, *ACS Nano* **2016**, *10*, 4652.

[99] Z.-H. Lin, G. Zhu, Y. S. Zhou, Y. Yang, P. Bai, J. Chen, Z. L. Wang, *Angew. Chem., Int. Ed.* **2013**, *52*, 5065.

[100] Z. Li, J. Chen, J. Yang, Y. Su, X. Fan, Y. Wu, C. Yu, Z. L. Wang, *Energy Environ. Sci.* **2015**, *8*, 887.

[101] Z. Wen, J. Chen, M.-H. Yeh, H. Guo, Z. Li, X. Fan, T. Zhang, L. Zhu, Z. L. Wang, *Nano Energy* **2015**, *16*, 38.

[102] H. Zhang, Y. Yang, Y. Su, J. Chen, C. Hu, Z. Wu, Y. Liu, C. P. Wong, Y. Bando, Z. L. Wang, *Nano Energy* **2013**, *2*, 693.

[103] S. Ornes, *Proc. Natl. Acad. Sci. USA* **2016**, *113*, 11059.

[104] L. Atzori, A. Iera, G. Morabito, *Comput. Networks* **2010**, *54*, 2787.

[105] S. P. Banerjee, D. L. Woodard, *J. Pattern Recognit. Res.* **2012**, *7*, 116.

[106] F. Monrose, A. D. Rubin, *Future Gener. Comput. Syst.* **2000**, *16*, 351.

[107] R. J. Spillane, *Tech. Discl. Bull.* **1975**, *17*.

[108] J. Chen, G. Zhu, J. Yang, Q. Jing, P. Bai, W. Yang, X. Qi, Y. Su, Z. L. Wang, *ACS Nano* **2015**, *9*, 105.

[109] S. Li, W. Peng, J. Wang, L. Lin, Y. Zi, G. Zhang, Z. L. Wang, *ACS Nano* **2016**, *10*, 7973.

[110] C. Wu, W. Ding, R. Liu, J. Wang, A. C. Wang, J. Wang, S. Li, Y. Zi, Z. L. Wang, *Mater. Today* **2018**, *21*, 216.

[111] W. Ding, C. Wu, Y. Zi, H. Zou, J. Wang, J. Cheng, A. C. Wang, Z. L. Wang, *Nano Energy* **2018**, *47*, 566.

[112] X. Pu, H. Guo, J. Chen, X. Wang, Y. Xi, C. Hu, Z. L. Wang, *Sci. Adv.* **2017**, *3*, e1700694.

[113] H. Guo, X. Pu, J. Chen, Y. Meng, M.-H. Yeh, G. Liu, Q. Tang, B. Chen, D. Liu, S. Qi, C. Wu, C. Hu, J. Wang, Z. L. Wang, *Sci. Robot.* **2018**, *3*.

[114] Y. Yang, G. Zhu, H. Zhang, J. Chen, X. Zhong, Z.-H. Lin, Y. Su, P. Bai, X. Wen, Z. L. Wang, *ACS Nano* **2013**, *7*, 9461.

[115] J. Bae, J. Lee, S. Kim, J. Ha, B.-S. Lee, Y. Park, C. Choong, J.-B. Kim, Z. L. Wang, H.-Y. Kim, J.-J. Park, U. I. Chung, *Nat. Commun.* **2014**, *5*, 4929.

[116] J. Wang, W. Ding, L. Pan, C. Wu, H. Yu, L. Yang, R. Liao, Z. L. Wang, *ACS Nano* **2018**, *12*, 3954.

[117] B. Chen, Y. Yang, Z. L. Wang, *Adv. Energy Mater.* **2018**, *8*, 1702649.

[118] L. Zheng, Z.-H. Lin, G. Cheng, W. Wu, X. Wen, S. Lee, Z. L. Wang, *Nano Energy* **2014**, *9*, 291.

[119] H. R. Zhu, W. Tang, C. Z. Gao, Y. Han, T. Li, X. Cao, Z. L. Wang, *Nano Energy* **2015**, *14*, 193.

[120] M.-H. Yeh, L. Lin, P.-K. Yang, Z. L. Wang, *ACS Nano* **2015**, *9*, 4757.

[121] Y. Xi, J. Wang, Y. Zi, X. Li, C. Han, X. Cao, C. Hu, Z. Wang, *Nano Energy* **2017**, *38*, 101.

[122] Y. Yang, H. Zhang, R. Liu, X. Wen, T.-C. Hou, Z. L. Wang, *Adv. Energy Mater.* **2013**, *3*, 1563.

[123] X. Wen, W. Yang, Q. Jing, Z. L. Wang, *ACS Nano* **2014**, *8*, 7405.

[124] L. M. Zhang, C. B. Han, T. Jiang, T. Zhou, X. H. Li, C. Zhang, Z. L. Wang, *Nano Energy* **2016**, *22*, 87.

[125] Z. L. Wang, *Nature* **2017**, *542*, 159.

[126] G. Zhu, Y. Su, P. Bai, J. Chen, Q. Jing, W. Yang, Z. L. Wang, *ACS Nano* **2014**, *8*, 6031.

[127] L. Xu, Y. Pang, C. Zhang, T. Jiang, X. Chen, J. Luo, W. Tang, X. Cao, Z. L. Wang, *Nano Energy* **2017**, *31*, 351.

[128] J. Chen, J. Yang, Z. Li, X. Fan, Y. Zi, Q. Jing, H. Guo, Z. Wen, K. C. Pradel, S. Niu, Z. L. Wang, *ACS Nano* **2015**, *9*, 3324.

[129] X. Wang, S. Niu, Y. Yin, F. Yi, Z. You, Z. L. Wang, *Adv. Energy Mater.* **2015**, *5*, 1501467.

[130] L. Xu, T. Jiang, P. Lin, J. J. Shao, C. He, W. Zhong, X. Y. Chen, Z. L. Wang, *ACS Nano* **2018**, *12*, 1849.

[131] T. Jiang, Y. Yao, L. Xu, L. Zhang, T. Xiao, Z. L. Wang, *Nano Energy* **2017**, *31*, 560.

[132] C. Wu, R. Liu, J. Wang, Y. Zi, L. Lin, Z. L. Wang, *Nano Energy* **2017**, *32*, 287.

[133] A. Li, Y. Zi, H. Guo, Z. L. Wang, F. M. Fernández, *Nat. Nanotechnol.* **2017**, *12*, 481.

[134] C. B. Han, T. Jiang, C. Zhang, X. Li, C. Zhang, X. Cao, Z. L. Wang, *ACS Nano* **2015**, *9*, 12552.

[135] J. Nie, J. Ren, J. Shao, C. Deng, L. Xu, X. Chen, M. Li, Z. L. Wang, *ACS Nano* **2018**, *12*, 1491.

[136] J. Cheng, W. Ding, Y. Zi, Y. Lu, L. Ji, F. Liu, C. Wu, Z. L. Wang, *Nat. Commun.* **2018**, *9*, 3733.

[137] G. Q. Gu, C. B. Han, C. X. Lu, C. He, T. Jiang, Z. L. Gao, C. J. Li, Z. L. Wang, *ACS Nano* **2017**, *11*, 6211.

[138] X. Chen, T. Jiang, Y. Yao, L. Xu, Z. Zhao, Z. L. Wang, *Adv. Funct. Mater.* **2016**, *26*, 4906.

[139] X. Chen, Y. Wu, A. Yu, L. Xu, L. Zheng, Y. Liu, H. Li, Z. L. Wang, *Nano Energy* **2017**, *38*, 91.

[140] L. Zheng, Y. Wu, X. Chen, A. Yu, L. Xu, Y. Liu, H. Li, Z. L. Wang, *Adv. Funct. Mater.* **2017**, *27*, 1606408.

[141] C. Li, Y. Yin, B. Wang, T. Zhou, J. Wang, J. Luo, W. Tang, R. Cao, Z. Yuan, N. Li, X. Du, C. Wang, S. Zhao, Y. Liu, Z. L. Wang, *ACS Nano* **2017**, *11*, 10439.

[142] Y. Zi, C. Wu, W. Ding, X. Wang, Y. Dai, J. Cheng, J. Wang, Z. Wang, Z. L. Wang, *Adv. Funct. Mater.* **2018**, *28*, 1800610.

[143] S. Li, S. Wang, Y. Zi, Z. Wen, L. Lin, G. Zhang, Z. L. Wang, *ACS Nano* **2015**, *9*, 7479.

[144] S. Li, D. Zhang, X. Meng, Q.-A. Huang, C. Sun, Z. L. Wang, *Energy Storage Mater.* **2018**, *12*, 17.

[145] M. Xia, J. Nie, Z. Zhang, X. Lu, Z. L. Wang, *Nano Energy* **2018**, *47*, 43.